

Estimating Uncertainty in Neural Networks for Cardiac MRI Segmentation: A Benchmark Study

Matthew Ng, Fumin Guo, Labonny Biswas, Steffen E. Petersen, Stefan K. Piechnik, Stefan Neubauer, Graham Wright

Abstract—Objective: Convolutional neural networks (CNNs) have demonstrated promise in automated cardiac magnetic resonance image segmentation. However, when using CNNs in a large real-world dataset, it is important to quantify segmentation uncertainty and identify segmentations which could be problematic. In this work, we performed a systematic study of Bayesian and non-Bayesian methods for estimating uncertainty in segmentation neural networks.

Methods: We evaluated Bayes by Backprop, Monte Carlo Dropout, Deep Ensembles, and Stochastic Segmentation Networks in terms of segmentation accuracy, probability calibration, uncertainty on out-of-distribution images, and segmentation quality control.

Results: We observed that Deep Ensembles outperformed the other methods except for images with heavy noise and blurring distortions. We showed that Bayes by Backprop is more robust to noise distortions while Stochastic Segmentation Networks are more resistant to blurring distortions. For segmentation quality control, we showed that segmentation uncertainty is correlated with segmentation accuracy for all the methods. With the incorporation of uncertainty estimates, we were able to reduce the percentage of poor segmentation to 5% by flagging 31–48% of the most uncertain segmentations for manual review, substantially lower than random review without using neural network uncertainty (reviewing 75–78% of all images).

Conclusion: This work provides a comprehensive evaluation of uncertainty estimation methods and showed that Deep Ensembles outperformed other methods in most cases.

Significance: Neural network uncertainty measures can help identify potentially inaccurate segmentations and alert users for manual review.

Index Terms—Cardiac MRI segmentation, segmentation qual-

Corresponding authors: Fumin Guo (fguo@hust.edu.cn), Matthew Ng (matthewng.ng@mail.utoronto.ca)

M Ng and G Wright are with the Physical Sciences Platform at Sunnybrook Research Institute and Department of Medical Biophysics, University of Toronto, Toronto, ON, Canada.

F Guo is with the Wuhan National Laboratory for Optoelectronics and Biomedical Engineering, Huazhong University of Science and Technology, Wuhan, China, and Physical Sciences Platform at Sunnybrook Research Institute and Department of Medical Biophysics, University of Toronto, Toronto, ON, Canada.

L Biswas is with the Physical Sciences Platform, Sunnybrook Research Institute, Toronto, ON, Canada.

SE Petersen is with the William Harvey Research Institute, NIHR Barts Biomedical Research Centre, Queen Mary University of London, UK and Barts Heart Centre, St Bartholomew's Hospital, Barts Health NHS Trust, West Smithfield, London, UK.

SK Piechnik and S Neubauer are with the Division of Cardiovascular Medicine, Oxford NIHR Biomedical Research Centre, Radcliffe Department of Medicine, University of Oxford, Oxford, UK.

Copyright ©2022 IEEE. Personal use of this material is permitted. Permission from IEEE must be obtained for all other uses, in any current or future media, including reprinting/republishing this material for advertising or promotional purposes, creating new collective works, for resale or redistribution to servers or lists, or reuse of any copyrighted component of this work in other works. DOI: 10.1109/TBME.2022.3232730

ity control, Bayesian neural networks, uncertainty

I. INTRODUCTION

CARDIAC magnetic resonance imaging (MRI) is the gold standard for evaluating cardiac function due to its excellent soft tissue contrast, high spatial and temporal resolution, and non-ionizing radiation [1]. Segmentation of cardiac structures such as the left ventricle cavity, left ventricle myocardium, and right ventricle cavity is required as a first step to quantify clinically relevant imaging biomarkers, such as the left ventricle ejection fraction and myocardial mass. Recently, convolutional neural networks (CNNs) have demonstrated promise for automatic cardiac MR image segmentation [2], [3] and may facilitate the development of efficient cardiac MR image processing pipelines for research and clinical use. However, when using a CNN in an automated image analysis pipeline, it is important to automatically identify which segmentations are problematic and require further manual inspection. This may improve workflow efficiency by focusing only on problematic cases, avoiding the review of all images and reducing errors in downstream analysis.

This problem has been referred to as *segmentation quality control* and is closely related to the task of anomaly detection or out-of-distribution detection [4]. While there are several approaches to this problem (e.g., using a dedicated quality control module [5]), in this work, we focus on the approach of using predictive uncertainty estimates of a segmentation model to solve this problem. The main idea here is that segmentation outputs with low uncertainty are *likely* correct while those with high uncertainty are *likely* problematic. While several studies have attempted to estimate CNN segmentation uncertainty, most of them used Monte Carlo (MC) Dropout or Deep Ensembles. However, there are some limitations associated with these methods, which motivates us to explore other algorithms. For example, when using a fixed dropout rate in MC Dropout, the model uncertainty does not decrease when training data is increased. This is potentially problematic since model uncertainty should approach zero in the limit of infinite training data [6]. For Deep Ensembles, it is not clear *why* this method generates well-calibrated uncertainty estimates. While Deep Ensembles was shown to learn diverse functions [7], recent work [8] has shown that ensemble diversity does not explain the improved uncertainty estimates on out-of-distribution data. In addition, in previous studies, evaluation of these algorithms was mostly limited to correlations between the predictive uncertainty and segmentation accuracy or metrics measuring

how uncertainty can be used to improve segmentation [9], [10], [11]. There is a need to have a proper benchmark and metrics to evaluate uncertainty from different methods. In this work, we performed a systematic evaluation of several Bayesian and non-Bayesian approaches for uncertainty estimation. In particular, we evaluated Bayes by Backprop, MC Dropout, Deep Ensembles, and Stochastic Segmentation Networks based on segmentation accuracy, probability calibration, uncertainty on out-of-distribution datasets, and finally, we demonstrated the utility of these methods for segmentation quality control.

A. Uncertainty in Neural Networks

Uncertainty is usually classified into epistemic uncertainty or aleatoric uncertainty [12]. Epistemic or model uncertainty is uncertainty in model parameters due to a finite amount of data. In contrast, aleatoric or data-dependent uncertainty is uncertainty due to the data itself and cannot be reduced even with more data. This distinction can be useful when thinking about sources of uncertainty; however, it is difficult to distinguish these two types in practice. Instead, we can think about modelling uncertainties in neural networks by learning a distribution of neural network weights or by learning a distribution of neural network outputs for each individual input [12]. Uncertainty from both types of models can be used and compared for downstream tasks.

Bayesian neural networks (BNNs) provide a theoretical framework for generating well-calibrated uncertainty estimates [13]. In BNNs, we are interested in learning the posterior distribution of the neural network weights instead of a maximum likelihood or maximum-a-posteriori estimate. A challenge in learning BNNs is that integration over the posterior is intractable in high dimensional space. As such, inference techniques such as stochastic variational inference are commonly used as approximation. Examples include variational dropout [14], MC Dropout [15], Bayes by Backprop [16], multiplicative normalizing flows [17], and Flipout [18]. Non-Bayesian methods for estimating uncertainty in neural networks include bootstrapping [19], Deep Ensembles [20], and Resampling Uncertainty Estimation [21]. These methods estimate changes to the neural network when it is trained on different samples from the same training distribution. Note that in Bayesian methods, uncertainty is learned during training and is tightly coupled to the model structure. In non-Bayesian methods, uncertainty is learned during training or estimated after training. Another approach to uncertainty estimation is to directly learn a distribution of neural network outputs (and/or intermediate feature maps) instead of the weights. This is usually achieved by parameterizing the output distribution and learning the parameters during training as shown in [12].

B. Related Studies

The majority of investigations of BNNs used MC Dropout to approximate the posterior distribution of the weights and exploration of ways to evaluate the quality of uncertainty has been limited. Previous studies [9], [10], and [22] used MC Dropout for brain structure, brain tumour, and brain tumour cavity segmentation. These studies reported positive

correlations between segmentation accuracy and uncertainty measures. Nair et al. [23] compared different uncertainty measures in brain lesion segmentation and showed that uncertainty measures can be used to improve lesion detection accuracy. Sander et al. [11] applied MC Dropout for cardiac MRI segmentation and showed that training a CNN using a Brier loss or cross-entropy loss produced well-calibrated pixel-wise segmentation uncertainty, and correcting uncertain pixels can improve segmentation results consistently. Devries et al. [24] used MC Dropout and non-Bayesian methods to generate skin lesion segmentation and segmentation uncertainty maps, which were then entered into another neural network to predict the Jaccard index of the segmentation. Hann et al. [25] estimated the quality of aortic MRI segmentation using an ensemble of neural networks and demonstrated improved segmentation accuracy with the use of these segmentation quality estimates. More recently, Jungo et al. [26] compared MC Dropout, Deep Ensembles, and auxiliary networks for predicting pixel-wise segmentation errors for two medical image segmentation tasks. In addition to segmentation probability calibration, they examined the overlap between segmentation uncertainty and errors, and the fraction of images which would benefit from uncertainty-guided segmentation correction. In a follow-up study [27], the authors compared different aggregation methods for uncertainty measures and their performance for segmentation failure detection. Similarly, Mehrtash et al. [28] compared MC Dropout and Deep Ensembles for CNNs trained with different loss functions in terms of probability calibration and correlation between segmentation accuracy and uncertainty measures. However, these studies did not evaluate other Bayesian methods such as Bayes by Backprop and the performance of these methods on out-of-distribution datasets is unknown. Other methods such as Probabilistic U-net [29], PHiSeg [30], and Stochastic Segmentation Networks [31] estimate uncertainty by directly predicting a distribution of neural network outputs. These methods have been applied to brain and lung tumour segmentation and have shown to produce diverse outputs matching inter-observer manual segmentation variability. [32] presented a framework for segmentation quality control of cardiac T1 maps using the evidence lower bound scores from PHiSeg and a separate quality control neural network. While this showed great sensitivity and specificity for detecting poor segmentations, it is not clear how other algorithms would compare with PHiSeg for this task.

C. Contributions

In this work, we performed a systematic study of Bayesian and non-Bayesian neural networks for estimating uncertainty in the context of cardiac MRI segmentation. Our contributions are summarized as follows:

- 1) We compared MC Dropout and Deep Ensembles with Bayes by Backprop, which is a more theoretically justified algorithm for learning uncertainty in BNNs. We performed a comprehensive evaluation of these algorithms in terms of segmentation accuracy, probability calibration, uncertainty on out-of-distribution datasets, and segmentation quality control.

- 2) We evaluated MC Dropout, Deep Ensembles, Bayes by Backprop, and Stochastic Segmentation Networks on cardiac MRI datasets with various degrees of noise, blurring, and stretching distortions to mimic complex clinical scenarios and to investigate the relationships between image distortions and neural network uncertainty estimates. We showed that Bayes by Backprop is more robust to noise distortions while Stochastic Segmentation Networks are more resistant to blurring distortions.
- 3) We introduced a novel area-under-the-curve metric for quantifying algorithm performance on segmentation quality control. We showed that with the use of Deep Ensemble uncertainty estimates, 31–48% of the most uncertain segmentations need to be reviewed to reduce the percentage of poor segmentations to 5%, whereas ~80% of the results need to be reviewed when neural network uncertainty measures are not used.

We hope this work will serve as a benchmark for evaluating uncertainty in cardiac MRI segmentation and inspire further work on uncertainty estimation in medical image segmentation.

II. METHODS

A. Bayesian Neural Networks

Given a dataset of N images $\mathbf{X} = \{\mathbf{x}_i\}$, $i \in [1, N]$, and the corresponding manual segmentation $\mathbf{Y} = \{y_i\}$ with C classes, we fit a neural network parameterized by weights \mathbf{w} to perform segmentation. In BNNs, we are interested in learning the posterior distribution of the weights $p(\mathbf{w}|\mathbf{X}, \mathbf{Y})$, instead of a maximum likelihood or maximum-a-posteriori estimate. This posterior distribution represents uncertainty in the weights, which could be propagated to calculate uncertainty in the predictions [33]. In addition, BNNs have been shown to be able to improve the generalizability of neural networks [33].

A challenge in learning BNNs is that calculating the posterior is intractable due to the high dimensionality of the weights. Variational inference [34] is a scalable technique that aims to learn an approximate posterior distribution of the weights $q(\mathbf{w})$ by minimizing the Kullback-Leibler (KL) divergence between the approximate and true posterior. This is equivalent to maximizing the evidence lower bound as follows:

$$\arg \max_{q(\mathbf{w})} \mathbb{E}_{q(\mathbf{w})} [\log p(\mathbf{Y}|\mathbf{X}, \mathbf{w})] - \lambda \cdot \text{KL}[q(\mathbf{w})||p(\mathbf{w})], \quad (1)$$

where $\mathbb{E}_{q(\mathbf{w})}[\cdot]$ denotes expectation over the approximate posterior $q(\mathbf{w})$, $\log p(\mathbf{Y}|\mathbf{X}, \mathbf{w})$ is the log-likelihood of the training data with given weights \mathbf{w} , $p(\mathbf{w})$ represents the prior distribution of \mathbf{w} , and $\text{KL}[\cdot]$ is the KL divergence between two probability distributions weighted by a hyperparameter $\lambda > 0$.

State-of-the-art segmentation neural networks such as the U-net formulate image segmentation as a pixel classification problem. For each pixel $x_{i,j}$ in image \mathbf{x}_i , $i \in [1, N]$, $j \in \Omega$, the neural network generates a prediction $\hat{y}_{i,j}$ with probability $p(\hat{y}_{i,j} = c)$, $c \in [0, C - 1]$, through softmax activation of the features in the last layer. Assuming pixels are independent from each other, the log-likelihood of the training data in Eq.

(1) is given by:

$$\log p(\mathbf{Y}|\mathbf{X}, \mathbf{w}) = \sum_{i=1}^N \sum_{j \in \Omega} \sum_{c=0}^{C-1} [y_{i,j} = c] \cdot \log p(\hat{y}_{i,j} = c),$$

where $y_{i,j}$ is the manual label for pixel j in image x_i and $[\cdot]$ is the indicator function. In this setting, the log-likelihood is also the negative cross entropy between the manual segmentation and algorithm prediction. The prediction $\hat{\mathbf{y}}$ of a test image \mathbf{x} is generated by marginalizing out the weights of the neural network, i.e.,

$$p(\hat{\mathbf{y}}|\mathbf{x}) = \mathbb{E}_{q(\mathbf{w})} [p(\hat{\mathbf{y}}|\mathbf{x}, \mathbf{w})], \quad (2)$$

where $p(\hat{\mathbf{y}}|\mathbf{x}, \mathbf{w})$ denotes the prediction of an image \mathbf{x} given network weights \mathbf{w} . In the following sections, we introduce methods for estimating an approximate posterior $q(\mathbf{w})$ for the weights of a BNN.

1) *Bayes by Backprop*: One way to parameterize the approximate posterior $q(\mathbf{w})$ is to use a fully factorized Gaussian. In a fully factorized Gaussian, each weight w in \mathbf{w} is independent from others and follows its own Gaussian distribution with mean μ and standard deviation σ . To ensure $\sigma > 0$ and training stability, σ is parameterized by a real number ρ , i.e., $\sigma = \text{softplus}(\rho) = \ln(1 + e^\rho)$. The prior distribution $p(\mathbf{w})$ is usually chosen as a fully factorized Gaussian with mean $\mu_{\text{prior}}\mathbf{I}$ and covariance $\sigma_{\text{prior}}\mathbf{I}$, i.e., $p(\mathbf{w}) = \mathcal{N}(\mu_{\text{prior}}\mathbf{I}, \sigma_{\text{prior}}\mathbf{I})$, where \mathbf{I} represents an identity matrix. Gradient updates can be performed using the “reparameterization trick”. The training procedure is known as Bayes by Backprop (BBB) [16] and is briefly described below:

- (1) For each weight w , sample $\epsilon \sim \mathcal{N}(0, 1)$ and set $w = \mu + \text{softplus}(\rho) \cdot \epsilon$.
- (2) Calculate the loss based on Eq. (1), i.e., $-\log p(\mathbf{Y}|\mathbf{X}, \mathbf{w}) + \lambda \cdot \text{KL}[q(\mathbf{w})||\mathcal{N}(\mu_{\text{prior}}\mathbf{I}, \sigma_{\text{prior}}\mathbf{I})]$.
- (3) Update μ and ρ through gradient descent.

After training, each weight w can be sampled from $\mathcal{N}(\mu, \sigma)$, which is then used to generate the segmentation predictions following Eq. (2).

2) *MC Dropout*: MC Dropout (MCD) [15] is another commonly used method for learning BNNs because it is straightforward to implement and does not require additional parameters or weights. MCD can be interpreted as choosing the approximate posterior distribution $q(\mathbf{w})$ to be a mixture of two Gaussians with minimal variances, e.g., one at 0 and the other at the weight w . Dropout is applied during training and testing to sample weights from $q(\mathbf{w})$. In this method, the dropout rate is a hyperparameter chosen empirically based on a validation dataset. The dropout rate defines the amount of uncertainty in the weights and is fixed throughout network training and testing.

B. Deep Ensembles

In addition to BNNs, we characterized and evaluated uncertainty estimates using an ensemble of neural networks, i.e., Deep Ensembles [20]. Deep Ensembles consist of multiple neural networks trained using the same data (or different subsets of the same data) with different random initializations.

Combining these models in an ensemble has been shown to produce well-calibrated probabilities in computer vision tasks and the variability between the model predictions can be used to calculate predictive uncertainty. This non-Bayesian method was inspired by the idea of bootstrapping, where stochasticity in the sampling of the training data and training algorithm define model uncertainty. This approach differs from Bayesian methods since it does not require approximation of the posterior distribution of the weights.

C. Stochastic Segmentation Networks

Another method for uncertainty estimation involves predicting a distribution over the neural network logits before transforming them into probabilities. Since standard segmentation neural networks output pixelwise logits, a simple method is to assume a Gaussian distribution of the logits and that each pixel is independent from others, i.e., for each image \mathbf{x} , the neural network predicts logits $\eta \sim \mathcal{N}(\mu(\mathbf{x}), \Sigma(\mathbf{x}))$, where $\mu(\mathbf{x}) \in \mathbb{R}^{|\Omega|C}$ is the mean logit and $\Sigma(\mathbf{x}) \in \mathbb{R}^{|\Omega|C \times |\Omega|C}$ is a diagonal covariance matrix [12]. Stochastic Segmentation Networks (SSNs) [31] improved this method by using a low rank multivariate normal distribution on the pixelwise logits to model the dependencies between pixels in an image. In particular, SSNs use $\Sigma(\mathbf{x}) = PP^T + D$, where $P \in \mathbb{R}^{|\Omega|C \times R}$ is a low rank matrix and $D \in \mathbb{R}^{|\Omega|C \times |\Omega|C}$ is a diagonal matrix.

D. Algorithm Evaluation

We evaluated the uncertainty estimation algorithms based on three aspects: (1) segmentation accuracy and probability calibration; (2) uncertainty on out-of-distribution datasets; and (3) application of uncertainty estimates for segmentation quality control. The purposes of these evaluations are as follows:

- (1) We show that BNNs can provide segmentation accuracies that are similar to or higher than plain or point estimate neural networks. In addition, predicted segmentation probabilities should be well-calibrated, i.e., a pixel with predicted probability of 60% belonging to the myocardium is 60% myocardium according to some ground truth. From a frequentist perspective, this means that out of all predictions with 60% probability, 60% of the predictions are correct.
- (2) We measure segmentation uncertainty on out-of-distribution data to validate that the uncertainty measures perform as expected, i.e., uncertainty should increase when test datasets substantially differ from training datasets.
- (3) We expect uncertainty measures to be useful in identifying problematic segmentations that require manual editing.

We used the following metrics for these evaluations:

1) *Segmentation Accuracy*: We calculated the algorithm segmentation accuracy using Dice similarity coefficient, average symmetric surface distance (ASSD), and Hausdorff distance (HD), as previously described [2].

2) *Probability Calibration*: These metrics measure how closely the neural network segmentation probabilities match the manual segmentation probabilities on a per-pixel basis.

Following the notation in Sec. II-A, let \hat{y}_j and y_j denote the prediction and manual label of pixel j in a given image, $j \in \Omega$, respectively. We use $p(\hat{y}_j = c)$ to denote the average per-pixel probability from the samples of the neural network, i.e., $p(\hat{y}_j = c) = \mathbb{E}_{q(\mathbf{w})}[p(\hat{y}_j = c|\mathbf{w})]$. Negative log-likelihood (NLL) measures how well the learned model fits the observed (testing) data and is calculated as follows:

$$\text{NLL} = \sum_{j \in \Omega} \sum_{c=0}^{C-1} [y_j = c] \cdot \log p(\hat{y}_j = c).$$

Note that NLL is sensitive to tail probabilities; that is, a model that generates low probability for the correct class is heavily penalized.

Brier score (BS) [35] is a proper scoring rule used to measure probability calibration. It measures the mean squared error between the predicted and manual segmentation probabilities:

$$\text{BS} = \sum_{j \in \Omega} \sum_{c=0}^{C-1} [p(\hat{y}_j = c) - p(y_j = c)]^2.$$

A Brier score of 0 indicates that the model is perfectly calibrated.

3) *Predictive Uncertainty Measures*: Predictive uncertainty can be calculated from neural network predictions to indicate the degree of uncertainty of the outputs. This can be calculated per pixel or per structure/class.

a) *Pixelwise Uncertainty Measures*: Pixelwise uncertainty measures are calculated per pixel and averaged across all pixels in an image if an image-level measure is required. In this work, we used multi-class predictive entropy and multi-class mutual information as suggested to be superior in [36]:

- Multi-class Predictive Entropy measures the spread of probabilities across all the classes in the mean prediction, i.e.,

$$\sum_{j \in \Omega} \sum_{c=0}^{C-1} [-p(\hat{y}_j = c) \log p(\hat{y}_j = c)].$$

- Multi-class Mutual Information (MI) measures how different each sample is from the mean prediction and is calculated as:

$$\mathbb{E}_{q(\mathbf{w})} \left[\sum_{j \in \Omega} \sum_{c=0}^{C-1} p(\hat{y}_j = c|\mathbf{w}) \log p(\hat{y}_j = c|\mathbf{w}) - \sum_{j \in \Omega} \sum_{c=0}^{C-1} p(\hat{y}_j = c) \log p(\hat{y}_j = c) \right],$$

where $p(\hat{y}_j = c|\mathbf{w})$ denotes the prediction given a set of weights \mathbf{w} . MI is high if there are samples with both high and low confidence, and is low if all samples have low confidence or high confidence.

b) *Structural Uncertainty Measures*: We define two structural uncertainty measures, which quantify how different the prediction samples are for each structure in terms of Dice and ASSD.

- $\text{Dice}_{\text{WithinSamples}}$ (**Dicews**) = $\frac{1}{T} \sum_{i=1}^T \text{Dice}(\bar{S}, S_i)$
- $\text{ASSD}_{\text{WithinSamples}}$ (**ASSDws**) = $\frac{1}{T} \sum_{i=1}^T \text{ASSD}(\bar{S}, S_i)$,

where \bar{S} is the mean of the T segmentation predictions $S_i, i \in [1, T]$. We expect structural uncertainty measures to better align with common segmentation accuracy metrics because of their global image-level focus.

E. Datasets

1) *UK BioBank (UKBB)*: The UKBB dataset [37] consists of 4845 healthy volunteers. For each subject, 2D cine cardiac MR images were acquired on a 1.5T Siemens scanner using a bSSFP sequence under breath-hold conditions with ECG-gating (pixel size = 1.8-2.3 mm, slice thickness = 8 mm, number of slices = ~ 10 , number of phases = ~ 50). Manual segmentation of the left ventricle blood pool (LV), left ventricle myocardium (Myo), and right ventricle (RV) was performed on the end-diastolic (ED) and end-systolic (ES) phases by one of eight observers followed by random checks by an expert to ensure segmentation quality and consistency. The dataset was randomly split into 4173, 103, and 569 subjects for training, validation, and testing, respectively. We have permission to use the UKBB dataset through UK Biobank’s generic RTB approval from the NHS North West REC.

2) *Automated Cardiac Diagnosis Challenge (ACDC)*: The ACDC dataset [3] consists of 100 patients with one of five conditions: normal, myocardial infarction, dilated cardiomyopathy, hypertrophic cardiomyopathy, and abnormal right ventricle. 2D cine MR images were acquired using a bSSFP sequence on a 1.5T/3T Siemens scanner (pixel size = 0.7-1.9 mm, slice thickness = 5-10 mm, number of slices = 6-18, number of phases = 28-40). Manual segmentation was performed at ED and ES phases with approval by two experts. This dataset was used for testing only.

F. Training Details

We used a plain 2D U-net [38] for BBB, MCD, Deep Ensembles, and SSN. The plain U-net consisted of 10 layers with 3×3 filters and 2 layers with 1×1 convolutions followed by a softmax layer. The number of filters ranged from 32 to 512 from the top to the bottom layers.

For BBB, we experimented with different standard deviations of the prior distributions: $\sigma_{\text{prior}} = 0.1$ or 1.0 and different weights for the KL term: $\lambda = 0.1, 1.0, 10, 30$. These are commonly used hyperparameters in the literature [39], [16], [40]. For MCD, we added dropout on all layers or only on the middle layers of the U-net with different dropout rates: 0.5, 0.3, and 0.1. These settings effectively tuned the amount of uncertainty in the model. For both BBB and MCD, the final prediction was obtained by averaging the softmax probabilities of $T=50$ samples. For Deep Ensembles, we trained 10 plain U-net models separately using all the training data with different random initializations and averaged the softmax probabilities

of the 10 models. For SSN, we used a rank of 10 for the multivariate normal distribution of the logits, as suggested in [31]. More training details can be found in Supplementary Material Section I.

III. EXPERIMENTS AND RESULTS

To select the hyperparameters for each method, we chose the models with the lowest NLL on the validation dataset since NLL is directly related to segmentation accuracy and probability calibration. For BBB, $\lambda = 10$ and $\sigma_{\text{prior}} = 0.1$ achieved the best NLL on the validation dataset. For MCD, adding dropout in the middle layers with a dropout rate of 0.1 (MCD-0.1) performed the best. We also reported results for MC Dropout with a dropout rate of 0.5 in the middle layers (MCD-0.5), which is commonly used in the literature.

A. Segmentation Accuracy and Probability Calibration

As shown in Table I, Deep Ensembles performed the best in terms of segmentation accuracy and probability calibration. This was followed by BBB and MCD-0.1, which were comparable to the plain U-net. MCD-0.5 performed slightly worse than the other models. The differences of these methods compared to the plain U-net were small but mostly statistically significant except for some metrics between plain U-net and MCD-0.1 (Table I). These results indicate that Bayesian approaches or Deep Ensembles can yield similar, if not better, segmentation results compared to a plain U-net while providing uncertainty estimates at the same time. The tradeoff is that Deep Ensembles and BBB use more memory and computation time compared to a plain U-net.

Examples of predicted segmentation from all methods are shown in Supplementary Figure S1.

B. Uncertainty on Distorted Images

In order to validate uncertainty measures as indicators of “out-of-distribution” datasets, we applied the trained models to carefully generated test images with various magnitudes of distortions, including:

- adding Rician noise, as found in MR images [41], with magnitudes ranging from 0.05 to 0.10 (on normalized images with intensities ranging from 0 to 1),
- Gaussian blurring with a standard deviation of 1–4 pixels,
- deforming or stretching around LV, Myo, and RV.

Note that these distortions were not applied as part of data augmentation during training and these images were not seen by the neural networks. As such, we expected decreased segmentation accuracy and increased predictive uncertainty in images with greater magnitudes of distortions. Figure 1 shows examples of distorted images.

1) *Trends with Increasing Distortions*: Figure 2 and Supplementary Table S1 show that the segmentation accuracy decreased as the magnitude of the distortions (noise, Gaussian blur, stretch) was increased. This is expected since these types of distortions were not seen during training and increasing the magnitude of the distortions results in greater differences with the original training datasets.

TABLE I

SEGMENTATION ACCURACY AND PROBABILITY CALIBRATION OF THE PLAIN U-NET, U-NET WITH MC DROPOUT, BBB, DEEP ENSEMBLE, OR SSN ON $N=1138$ IMAGES FROM UKBB. \uparrow INDICATES HIGHER IS BETTER. \downarrow INDICATES LOWER IS BETTER. FORMAT: MEAN (STANDARD DEVIATION).

	Dice \uparrow			ASSD (mm) \downarrow			HD (mm) \downarrow			NLL \downarrow	BS \downarrow
	LV	Myo	RV	LV	Myo	RV	LV	Myo	RV	($\times 10^{-2}$)	($\times 10^{-3}$)
Plain U-net	.941(.038)	.882(.031)	.907(.043)	1.01(.38)	1.02(.43)	1.61(.69)	2.98(0.99)	3.83(1.39)	6.53(2.67)	1.11(.38)	1.67(.54)
BBB	.942(.037)*	.883(.030)*	.908(.043)*	1.00(.36)*	1.00(.30)*	1.60(.70)*	2.96(0.96)*	3.80(1.23) \dagger	6.39(2.59)*	1.10(.35)*	1.66(.53)*
MCD-0.1	.941(.037)*	.882(.030) \dagger	.907(.043)*	1.00(.36)*	1.01(.31) \dagger	1.61(.70) \dagger	2.97(0.97) \dagger	3.82(1.24) \dagger	6.49(2.59) \dagger	1.10(.36)*	1.66(.53)*
MCD-0.5	.940(.038)*	.879(.030)*	.906(.043)*	1.03(.38)*	1.04(.31)*	1.64(.69)*	3.05(1.03)*	3.95(1.29)*	6.64(2.61)*	1.13(.35)*	1.70(.53)*
Ensemble	.943(.037)*	.885(.030)*	.909(.043)*	0.98(.36)*	0.98(.29)*	1.57(.72)*	2.90(0.93)*	3.68(1.20)*	6.26(2.56)*	1.07(.35)*	1.63(.52)*
SSN	.940(.037)*	.882(.030) \dagger	.903(.043)*	1.03(.39)*	1.03(.32)*	1.65(.67)*	3.08(1.10)*	3.90(1.29)*	6.64(2.55)*	1.15(.33)*	1.73(.50)*

* statistically different compared to the Plain U-net (Wilcoxon signed-rank test, $p < 0.05$, $N = 1138$ images).

\dagger not statistically different compared to the Plain U-net (Wilcoxon signed-rank test, $p > 0.05$, $N = 1138$ images).

In addition, we observed that the predictive uncertainty increased (i.e., higher predictive entropy, mutual information, $ASSD_{WS}$, and lower $Dice_{WS}$) with increasing magnitude of distortions but this decreased after a certain threshold, as shown in Figure 2. This was the case for Deep Ensembles, BBB, MCD, and SSN on images with noise and blurring distortions but not with stretching. For example, for BBB, the median predictive entropy for images with slight, moderate, and large additional noise was 1.66×10^{-2} , 1.95×10^{-2} , and 1.23×10^{-2} , respectively. Similarly, the median $ASSD_{WS}$ was 0.40, 3.40, and 0.71 mm for images with slight, moderate, and large amount of blurring, respectively (Supplementary Table S3). Figure 1 and Supplementary Figures S2-S4 show examples of segmentation predictions and uncertainty (predictive entropy, mutual information) for all the methods on images with increasing noise, blurring, and stretching.

While the increasing predictive uncertainty associated with increasing magnitude of distortions was expected, the decrease in predictive uncertainty after a threshold in cases of noise and blurring distortions is surprising. Specifically, for images that were highly distorted, all pixels were classified as background with low uncertainty (Figure 1, bottom row). Although this seems correct when only given the labeling choices of background, LV, Myo, and RV, we argue that the distorted pixels are markedly different from the background pixels in the training images and therefore, should have high uncertainty nonetheless. This is a limitation of all the uncertainty models tested and may be improved using more expressive posteriors.

Another observation is that the uncertainty measures began to fail/decrease when dramatic segmentation errors occurred, as shown in Figure 2. This suggests that other heuristics or algorithms such as those presented in [42] can be used to complement the uncertainty measures when trying to detect inaccurate segmentations. For example, segmentation with a non-circular LV blood pool or a blood volume < 50 mL is highly problematic and may indicate poor segmentation.

2) *Comparison between Deep Ensembles, BBB, MC Dropout, and SSN*: In terms of segmentation accuracy and probability calibration, BBB was more robust to noise distortions compared to the other methods. Specifically, BBB showed higher Dice and lower ASSD for LV, lower NLL and BS on images with greater noise distortions (Figure 1, rows 3-5 and Supplementary Tables S1 and S2, degree of distortion = 2, 3, 4). SSN showed higher segmentation accuracy in cases of greater blurring while Deep Ensembles showed higher segmentation accuracy with stretching distortions compared

to the other methods (Figure 2 and Supplementary Table S1, degree of distortion = 3, 4). In the greatest noise, blurring, and stretching distortions tested, BBB, SSN, and Deep Ensembles had statistically higher segmentation accuracy and probability calibration, respectively, when compared to other methods (Supplementary Tables S1 and S2).

C. Uncertainty on Dataset Shift

To further validate the uncertainty measures, we applied the models trained on the UKBB dataset to a distinctly different ACDC dataset. We expect decreased segmentation accuracy and increased predictive uncertainty on the ACDC test dataset compared to the UKBB test dataset, due to the presence of cardiac pathologies on the ACDC dataset and slightly different acquisition parameters.

As shown in Figure 3, we observed decreased segmentation accuracy and increased predictive uncertainty compared to the UKBB test dataset. In terms of segmentation accuracy and probability calibration, the methods from the best to the worst are: Deep Ensembles, BBB, MCD-0.1, SSN, Plain U-net, and MCD-0.5, as shown in Figure 3 and Supplementary Table S4. While most metrics are statistically different, some metrics between the following pairs are not statistically different: Deep Ensembles vs BBB, MCD-0.1 vs SSN, SSN vs Plain U-net, and Plain U-net vs MCD-0.5. Supplementary Table S5 shows detailed results of the pairwise significance tests.

D. Correlations between Uncertainty and Segmentation Accuracy

To demonstrate the potential utility of uncertainty measures, we evaluated the Spearman rank correlation between uncertainty measures and segmentation accuracy. We used the rank correlation instead of linear correlation to reduce the effects of a potential non-linear relationship between the two quantities.

Supplementary Figure S5 shows that the uncertainty measure with the strongest correlation with ASSD was $ASSD_{WS}$ (Spearman correlation between 0.58 and 0.69) in the case of training and testing on the UKBB dataset (UKBB \rightarrow UKBB). This is not surprising since the $ASSD_{WS}$ calculation was similar to ASSD. Similar observations were obtained for training on the UKBB dataset and testing on the ACDC dataset (UKBB \rightarrow ACDC) although the correlations were slightly lower (Spearman correlation between 0.44 and 0.66). These correlations suggest that the $ASSD_{WS}$ uncertainty measure is useful in predicting the segmentation quality when manual

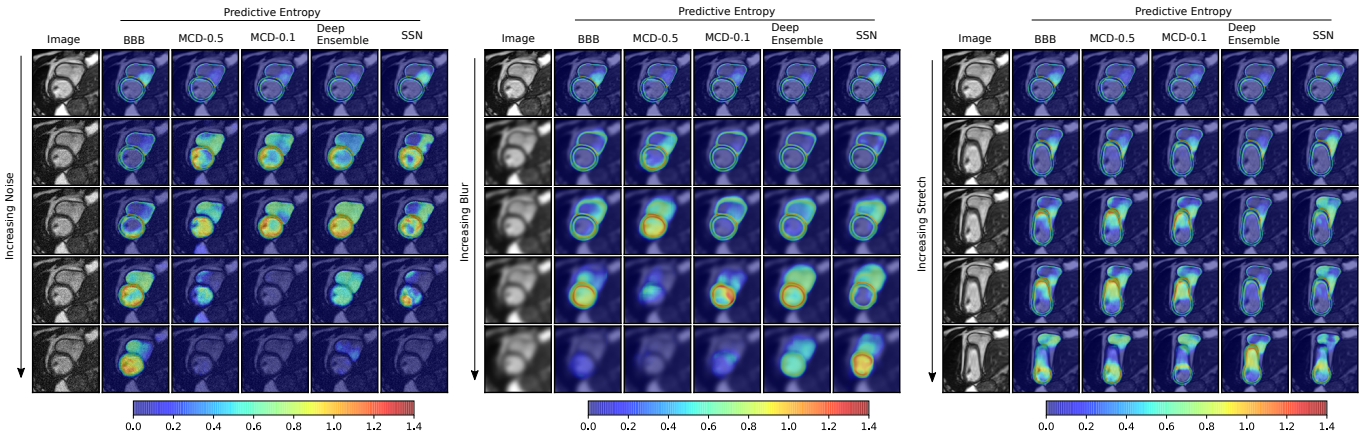


Fig. 1. Segmentation predictive entropy on images with increasing noise, blurring, and stretching. BBB showed the highest uncertainty on images with heavy noise (last two rows) while SSN showed the highest uncertainty on images with heaving blurring (last two rows); Deep Ensembles showed slightly higher uncertainty on images with heavy stretching compared to other methods. Reproduced with permission of UK Biobank ©.

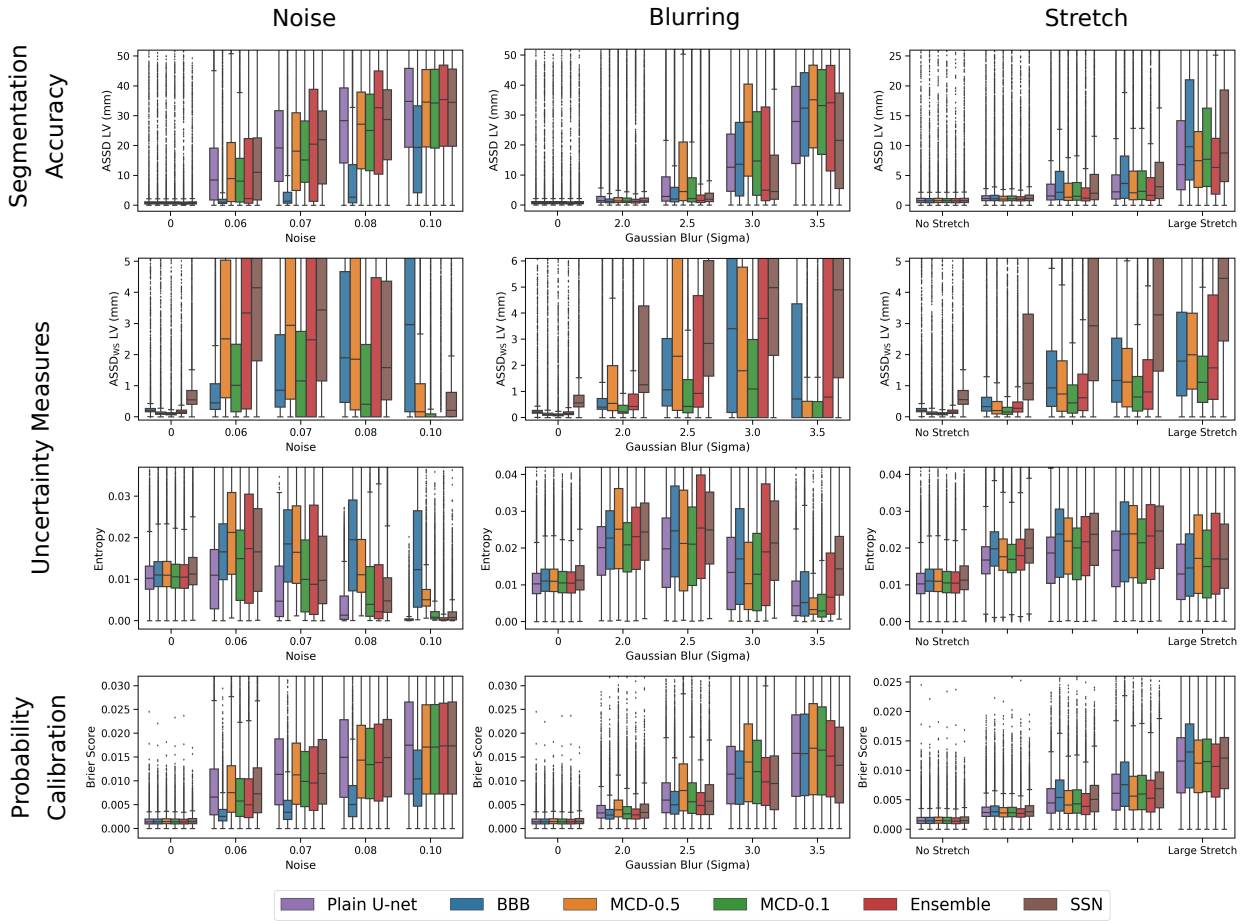


Fig. 2. Segmentation accuracy (ASSD LV), uncertainty measures (ASSD_{WS} LV, entropy), and probability calibration (Brier score) on images with increasing magnitude of noise, blurring, and stretching using a plain U-net, U-net with BBB, MC Dropout, Deep Ensemble, and SSN.

segmentation is not available. Other uncertainty measures such as MI or Dice_{WS} may correlate better with other segmentation quality metrics such as pixelwise accuracy or Dice (not explored in this work). They could also potentially be used as inputs to segmentation algorithms to improve segmentation performance.

rrior prediction samples, and the structural uncertainty measures for RV. The images with poor segmentation (toward the right side) had greater uncertainty as measured by Dice_{WS} and ASSD_{WS}. Note that posterior prediction samples are not related to inter- or intra-observer variability but rather show what the network has learned from given data.

Figure 4 shows representative segmentation results, poste-

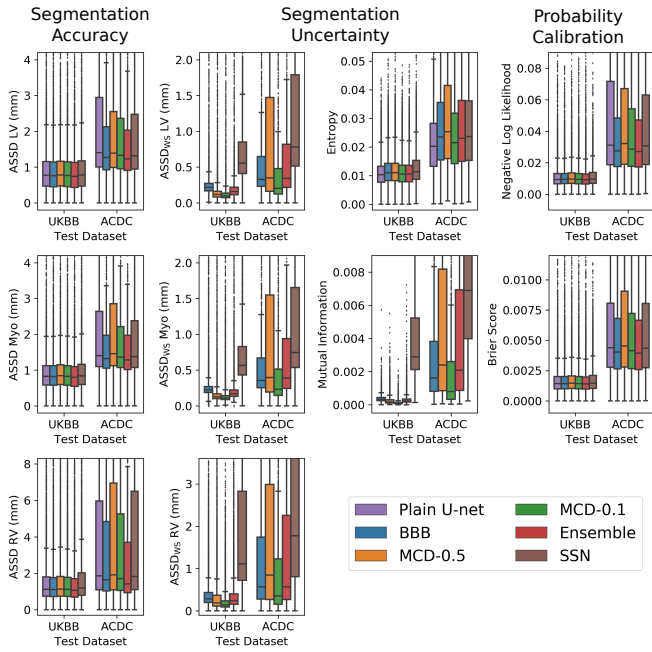


Fig. 3. Segmentation accuracy, predictive uncertainty, and probability calibration of models trained on the UKBB training dataset and tested on the UKBB and ACDC datasets.

E. Uncertainty for Segmentation Quality Control

In this section, we explored the use of predictive uncertainty estimates to flag potentially problematic segmentations that require manual review. We view this task as a classification problem and we aim to use uncertainty measures to classify segmentations as either good or poor.

While the common segmentation accuracy metrics (Dice, ASSD, HD) may not always correlate with true segmentation quality [3], there are no good alternatives to quantify segmentation quality. Having experts to manually determine whether an automated segmentation is good or not for a large dataset is time consuming and adds observer noise. Instead, we used thresholds on segmentation accuracies to achieve this. Based on our experience and discussions with our clinical collaborators, we believe that contour or surface distance is more indicative of inaccurate segmentations. As such, for each method, the predicted segmentation was considered as poor when the ASSD between the prediction and manual segmentation is greater than the ASSD between manual observers. We used inter-observer ASSD of 1.17 mm for LV, 1.19 mm for Myo, and 1.88 mm for RV, based on a recent relatively large-scale study [2]. We then evaluated how well the $ASDD_{WS}$ uncertainty measure could identify potentially poor segmentation.

To utilize the $ASDD_{WS}$ uncertainty measure, a threshold can be set such that any segmentation with uncertainty above the threshold is flagged for manual review. This would hopefully result in a decreased number of poor segmentation in the dataset. Figure 5 shows the fraction of images with poor segmentation remaining in the dataset and the fraction of images flagged for manual correction when the uncertainty thresholds were varied, i.e., (positives - true positives) vs (true

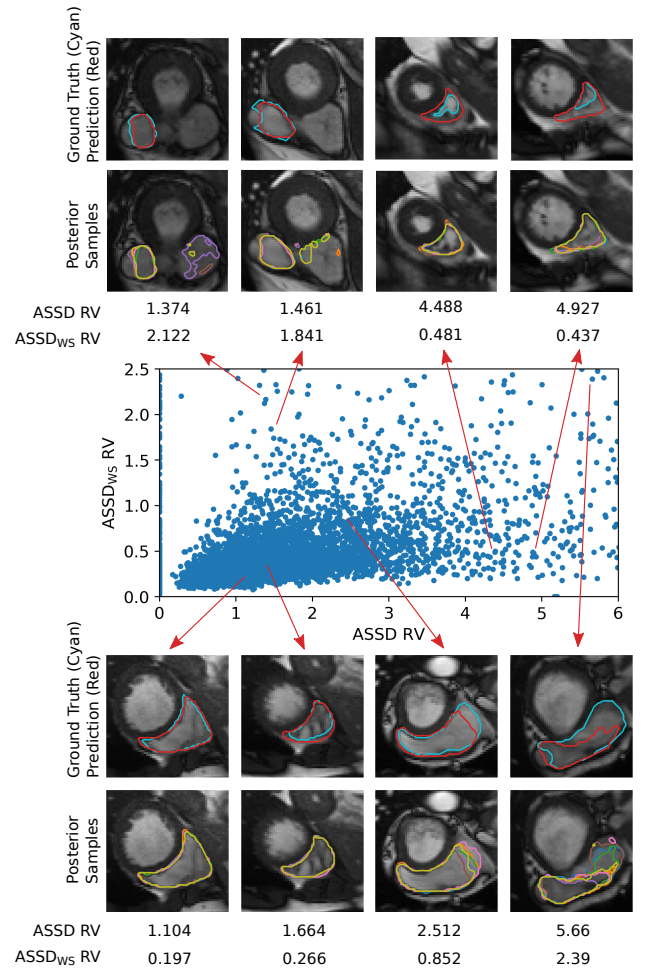


Fig. 4. A scatter plot showing the relationship between ASSD and $ASDD_{WS}$ using BBB. Images with manual and predicted segmentations, and posterior segmentation samples illustrate varying ASSD and $ASDD_{WS}$. Reproduced by kind permission of UK Biobank ©.

positives + false positives), where positive represents poor segmentation. As we decreased the uncertainty threshold (top left to bottom right in Figure 5), we flagged more images for manual correction and the number of images with poor segmentation was decreased. The first point on the curves corresponds to a threshold where none of the images are reviewed while the last point indicates that all the images are reviewed. This is similar to a receiver operating curve with the consideration that the total number of positives or images with poor predicted segmentation is different for each method. This allows for comparison between all the uncertainty estimation methods. In particular, a curve that is closer to the bottom left corner or has smaller area under the curve (AUC) indicates that the algorithm provides better initial segmentation and/or its uncertainty is a good indicator of segmentation accuracy. Figure 5 shows that all the methods performed similarly for detecting poor LV, Myo, and RV segmentation with Deep Ensembles having slightly lower AUC than the others.

The thresholds of the uncertainty measures for flagging images for manual review can be adjusted depending on the application. This approach provides a way to identify images to review and may result in substantial time savings. For example, using the $ASDD_{WS}$ uncertainty measure for the

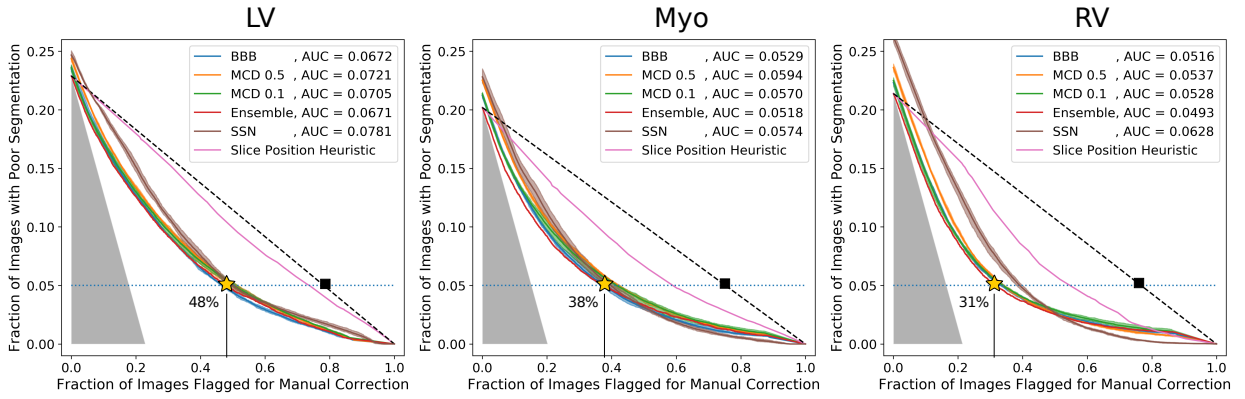


Fig. 5. Fraction of images with poor segmentation remaining (based on a threshold of ASSD between predicted and ground truth segmentation) after flagging images for manual correction using $ASSD_{WS}$ for BBB, MC Dropout, Deep Ensembles, and SSN. Dotted black lines indicate flagging images for manual correction randomly. Shaded area shows the ideal region where all images flagged for manual correction directly reduce the number of poor segmentations.

Deep Ensembles method, 48%, 38%, and 31% of the images required manual review in order to reduce the number of images with poor LV, Myo, or RV segmentation to 5% of the test dataset, respectively (Figure 5). In contrast, without using uncertainty measures and assuming no other information about the images is used, approximately 75% of the images need to be reviewed to achieve this goal. Furthermore, using the $ASSD_{WS}$ uncertainty measure resulted in more time savings compared to a naive approach based on slice position. Specifically, since the segmentation is usually worse at the base and/or apex, a naive approach for segmentation quality control is to first review all the most basal and apical slices, followed by the second-most basal and apical slices, and so on. We refer to this approach as using the slice position as a heuristic for segmentation quality control. As shown in Figure 5, using uncertainty measures is more advantageous than this naive approach as evidenced by a lower AUC and a smaller number of images to review to have 5% poor segmentation remaining. For example, for Myo, AUC for $ASSD_{WS}$ was 0.052 for Deep Ensembles and 0.080 for the slice position heuristic method; 38% of the total images require review when using the $ASSD_{WS}$ uncertainty measure compared to 59% when using the slice position heuristic. For a dataset of 10,000 subjects each with 10 slices and manual segmentation of 30 seconds per structure per slice [2], using the $ASSD_{WS}$ uncertainty measure results in ~ 940 hours of time savings compared to reviewing the images randomly, and ~ 580 hours of time savings compared to using the slice position heuristic.

IV. DISCUSSION

A. BBB vs MC Dropout vs Deep Ensembles vs SSN

In this work, we evaluated and compared different Bayesian and non-Bayesian methods for estimating uncertainty in neural networks for cardiac MRI segmentation. Here, we discuss the similarities and differences about how uncertainty is learned in these methods, what was learned after training, and relate these differences to the quality of the predictive uncertainties on out-of-distribution images.

While uncertainty in neural network parameters is learned automatically in BBB, this can be tuned by changing the

dropout rate in MCD. For the UKBB dataset, a small dropout rate of 0.1 in the middle layers performed better than the other MCD models in terms of segmentation accuracy and probability calibration. This is different from other studies which commonly used a dropout rate of 0.5 [43], [39] and may be because of the large amount of relatively uniform training data (i.e., images acquired following the same MR protocol in mainly healthy volunteers and labelled following the same guidelines). The dropout rate hyperparameters for MCD obtained through grid search correspond to the weight uncertainties learned by BBB to some extent. Figure 6 shows that the standard deviation of the weights learned by BBB is lower in the early layers and higher in the middle layers of the U-net. This is similar to MCD with no dropout in the early layers and with dropout on the middle layers. Having greater dropout rate in middle layers is common in other studies [39].

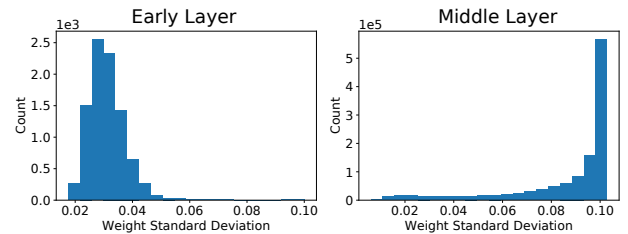


Fig. 6. Histogram of the standard deviations of weights in the early and middle layers learned by BBB.

The effect of using different dropout rate in MCD is shown in the experiments with dataset shift (Figure 3, Supplementary Tables S4 and S6, MCD-0.1 vs MCD-0.5). A dropout rate of 0.1 yielded higher segmentation accuracy but lower uncertainty whereas a dropout rate of 0.5 resulted in lower segmentation accuracy but higher predictive uncertainty. BBB was able to mitigate this issue by learning a mean and standard deviation for each weight, resulting in comparable or higher segmentation accuracy with moderate predictive uncertainties between MCD-0.1 and MCD-0.5 (Figure 3).

In Deep Ensembles, the uncertainty in the weights is not learned or tuned but instead stems from the random initialization of the weights and stochasticity of the training procedure.

Each model in the ensemble would learn a local minimum, which are combined to form a prediction and uncertainty estimate. Deep Ensembles outperformed BBB in terms of segmentation accuracy and probability calibration in most cases. This may be because the approximate posterior learned by BBB covered only one (or a few) mode(s) of the true posterior and a small neighbourhood around each mode, as opposed to multiple local modes in Deep Ensembles. Based on our observations, the histogram of the weights learned by each member in Deep Ensembles was very similar to each other. Techniques such as canonical correlation analysis may be used to compare the learned feature maps between different members of the ensemble to better understand model uncertainty [44].

The segmentation accuracy and uncertainty measures on images with increasing noise and blurring distortions provide some insights into the different algorithms tested. BBB outperformed the other methods in cases of noise distortions probably because the Gaussian distribution of the weights is complementary to the noise applied on the images (i.e., a Gaussian multiplied by an approximately-Gaussian distribution results in a Gaussian distribution). SSN outperformed the other methods in cases of blurring distortions since blurring is localized to a small region around each pixel and SSN models the distribution between pixels. Stretching distortions are complicated structural variations and in this case, Deep Ensembles performed the best by relying on weights from several local minima to model uncertainty. While these simple perturbations (noise, blurring, and stretching distortions) may not be realistic, they did highlight cases where BBB or SSN or Deep Ensembles are better than others. We tested these algorithms on the ACDC dataset for a more realistic comparison of the different algorithms.

Bayesian approaches and Deep Ensembles can be used to improve segmentation accuracy on slightly shifted datasets compared to the plain U-net (Supplementary Tables S4 and S5 show that there is a significant difference between the plain U-net and BBB/Deep Ensembles). While the segmentation accuracies on the ACDC test dataset using the models trained on UKBB dataset are lower than that obtained by training and testing on the ACDC dataset [3], the algorithms employed in this work may be combined with other techniques that are specifically designed to solve this problem, e.g., style augmentation or domain adversarial training [45], [46].

B. Pixelwise and Structural Uncertainty Measures

We introduced pixelwise and structural uncertainty measures to quantify the predictive uncertainty, and demonstrated the utility of these metrics for segmentation quality control. Both pixelwise and structural uncertainty measures can be used depending on the application. As the segmentation problem was formulated as pixel classification, pixelwise uncertainty measures are straightforward to obtain. These allow users to visualize which pixels and which areas are potentially problematic (Figure 1). However, segmentation is often performed at the image-level slice by slice. Therefore, image-level uncertainty measures for determining problematic segmentation are

also required. Accordingly, we showed that structural uncertainty measures were correlated with segmentation accuracy such as ASSD.

Other studies such as [36] evaluated uncertainty maps by comparing uncertainty and correctness at the per-pixel level. In contrast, we evaluated per-image uncertainty measures as a predictor of image-level segmentation quality, which is more reflective of the real-world scenario.

It is important to note that the predictive uncertainty measures reflect the neural network uncertainty, which is different from human uncertainty. An example is the image with heavy noise in the last row in Figure 1. It is expected that human observers can manually segment this image with low observer variability; however, since this image is very different from the training data, the neural networks were not able to generate a reasonable segmentation and yielded high predictive entropy and mutual information for the entire cardiac structure.

C. Segmentation Quality Control

We showed that the uncertainty measures have moderate to good correlations with segmentation accuracy. This could have been negatively affected by manual segmentation noise. Framing segmentation quality control as a binary classification problem instead of evaluating the correlations or predicting the segmentation accuracy alleviates the issue of noise in manual segmentation. In this regard, we defined poor segmentation using a threshold on ASSD between the predicted and manual segmentation. This definition was adopted based on discussions with our clinical collaborators; however, it can be modified depending on the application. For example, other segmentation accuracy metrics such as Hausdorff distance or misclassification area can be used and the framework for evaluating uncertainty measures developed in this work may be applied directly.

Other studies of segmentation quality control include directly predicting segmentation accuracy or comparing the predicted segmentation to a reference database. Alba et al. [47] trained a random forest classifier to predict a binary label of correct or incorrect segmentation. The examples of correct segmentation were generated using the manual delineation while the incorrect segmentations were obtained by deforming or translating the manual segmentations. Robinson et al. [48] used a 3D residual network to directly predict the Dice of a segmentation from an image-segmentation pair. The network was trained and tested on a dataset created using a random forest segmentation algorithm. Ruijsink et al. [42] trained a CNN for detecting images with artefacts or incorrect planning and then excluded these from the segmentation pipeline. [42] and [49] also trained classification models to predict whether a segmentation is good or poor. These classifiers are agnostic to how the segmentation was generated. However, these approaches depend on training with expected segmentation failures, which may be challenging to incorporate during training. In contrast, our approach used uncertainty measures to detect poor segmentation and is more explainable without these issues. Instead of using a learning algorithm to determine segmentation quality, we used model uncertainty

which emerges intrinsically during algorithm training. A slight limitation of our approach is that sampling during the testing phase required up to 50x more computation time compared to a single prediction but this may be accelerated through parallelization.

Additionally, some studies estimate the “similarity” of the test image and/or predicted segmentation with respect to the training data as a proxy for segmentation quality. For example, Gonzalez and Mukhopadhyay [50] used scores from a self-supervised task to detect out-of-distribution test images (which can then be assumed to have poor segmentation results). Galati and Zuluaga [51] trained a convolutional autoencoder to reconstruct segmentation maps. Then, the predicted segmentation is fed into the autoencoder and segmentation quality measures are calculated based on the predicted segmentation and reconstructed prediction. These generative modelling approaches represent a promising line of work and are quite different from the discriminative approaches used in this work. One advantage of [50] is that the algorithm does not require ground truth segmentation for training. However, in both approaches, the prediction of the segmentation itself is decoupled from the prediction of segmentation quality.

Finally, another approach for segmentation quality control is using a modified version of Reverse Classification Accuracy to predict the accuracy of an image-segmentation pair [52]. This approach requires a reference database with manual segmentation. Each reference image is registered to the test image and the associated manual segmentations are warped accordingly to generate potential segmentations of the test image. Segmentation quality is estimated by comparing the potential segmentations and algorithm segmentation. A limitation of this approach is that it requires long time to predict the segmentation quality, mainly due to the registration steps.

V. CONCLUSIONS

In this work, we compared Bayesian and non-Bayesian methods, namely BBB, MCD, Deep Ensembles, and SSN for segmentation accuracy, probability calibration, and uncertainty estimates in the context of cardiac MRI segmentation in cases of various distortions. We found that Deep Ensembles performed better in terms of segmentation accuracy and probability calibration on in-distribution and out-of-distribution datasets; BBB outperformed the other methods on images with noise distortions while SSN outperformed the others on images with blurring distortions. We showed that $ASSD_{WS}$ uncertainty measure was strongly correlated with the segmentation accuracy; using uncertainty measures can result in substantial time savings by reducing the number of images that needs manual review for segmentation quality control.

ACKNOWLEDGMENTS

This research has been conducted using the UK Biobank Resource under Application Number 2964. We acknowledge the use of the facilities of Compute Canada. This work was funded by Canadian Institutes of Health Research (CIHR) MOP: #93531, Ontario Research Fund and GE Healthcare. FG is supported by a Banting postdoctoral fellowship.

This work was partly funded by the European Union’s Horizon 2020 research and innovation programme under grant agreement No 825903 (euCanShare project). SEP acts as a paid consultant to Circle Cardiovascular Imaging Inc., Calgary, Canada and Servier. SEP acknowledges support from the National Institute for Health Research (NIHR) Biomedical Research Centre at Barts, from the SmartHeart EPSRC programme grant (EP/P001009/1) and the London Medical Imaging and AI Centre for Value-Based Healthcare. SEP acknowledges support from the CAP-AI programme, London’s first AI enabling programme focused on stimulating growth in the capital’s AI sector. SEP, SN and SKP acknowledge the British Heart Foundation for funding the manual analysis to create a cardiovascular magnetic resonance imaging reference standard for the UK Biobank imaging resource in 5000 CMR scans (PG/14/89/31194). This project was enabled through access to the Medical Research Council eMedLab Medical Bioinformatics infrastructure, supported by the Medical Research Council (MR/L016311/1).

REFERENCES

- [1] P. Peng, K. Lekadir, A. Gooya, L. Shao, S. E. Petersen, and A. F. Frangi, “A review of heart chamber segmentation for structural and functional analysis using cardiac magnetic resonance imaging,” *Magnetic Resonance Materials in Physics, Biology and Medicine*, vol. 29, no. 2, pp. 155–195, 2016.
- [2] W. Bai, M. Sinclair, G. Tarroni, O. Oktay, M. Rajchl, G. Vaillant, A. M. Lee, N. Aung, E. Lukaschuk, M. M. Sanghvi *et al.*, “Automated cardiovascular magnetic resonance image analysis with fully convolutional networks,” *Journal of Cardiovascular Magnetic Resonance*, vol. 20, no. 1, p. 65, 2018.
- [3] O. Bernard, A. Lalonde, C. Zotti, F. Cervenansky, X. Yang, P.-A. Heng, I. Cetin, K. Lekadir, O. Camara, M. A. G. Ballester *et al.*, “Deep learning techniques for automatic mri cardiac multi-structures segmentation and diagnosis: Is the problem solved?” *IEEE Transactions on Medical Imaging*, 2018.
- [4] C. M. Bishop, “Novelty detection and neural network validation,” *IEE Proceedings-Vision, Image and Signal processing*, vol. 141, no. 4, pp. 217–222, 1994.
- [5] F. Galati, S. Ourselin, and M. A. Zuluaga, “From accuracy to reliability and robustness in cardiac magnetic resonance image segmentation: A review,” *Applied Sciences*, vol. 12, no. 8, p. 3936, 2022.
- [6] I. Osband, “Risk versus uncertainty in deep learning: Bayes, bootstrap and the dangers of dropout,” in *Proceedings of the NIPS* 2016 Workshop on Bayesian Deep Learning*, 2016.
- [7] S. Fort, H. Hu, and B. Lakshminarayanan, “Deep ensembles: A loss landscape perspective,” *arXiv preprint arXiv:1912.02757*, 2019.
- [8] T. Abe, E. K. Buchanan, G. Pleiss, R. Zemel, and J. P. Cunningham, “Deep ensembles work, but are they necessary?” *arXiv preprint arXiv:2202.06985*, 2022.
- [9] A. G. Roy, S. Conjeti, N. Navab, and C. Wachinger, “Inherent brain segmentation quality control from fully convnet monte carlo sampling,” in *International Conference on Medical Image Computing and Computer-Assisted Intervention*, A. F. Frangi, J. A. Schnabel, C. Davatzikos, C. Alberola-López, and G. Fichtinger, Eds. Springer, 2018, pp. 664–672.
- [10] A. Jungo, R. Meier, E. Ermis, E. Herrmann, and M. Reyes, “Uncertainty-driven sanity check: Application to postoperative brain tumor cavity segmentation,” in *Medical Imaging with Deep Learning*, 2018.
- [11] J. Sander, B. D. de Vos, J. M. Wolterink, and I. Išgum, “Towards increased trustworthiness of deep learning segmentation methods on cardiac mri,” in *Medical Imaging 2019: Image Processing*, vol. 10949. International Society for Optics and Photonics, 2019, p. 1094919.
- [12] A. Kendall and Y. Gal, “What uncertainties do we need in bayesian deep learning for computer vision?” in *Advances in neural information processing systems*, 2017, pp. 5574–5584.
- [13] R. M. Neal, *Bayesian learning for neural networks*. Springer Science & Business Media, 2012, vol. 118.

- [14] D. P. Kingma, T. Salimans, and M. Welling, "Variational dropout and the local reparameterization trick," in *Advances in Neural Information Processing Systems*, 2015, pp. 2575–2583.
- [15] Y. Gal and Z. Ghahramani, "Dropout as a bayesian approximation: Representing model uncertainty in deep learning," in *international conference on machine learning*, 2016, pp. 1050–1059.
- [16] C. Blundell, J. Cornebise, K. Kavukcuoglu, and D. Wierstra, "Weight uncertainty in neural network," in *International Conference on Machine Learning*, 2015, pp. 1613–1622.
- [17] C. Louizos and M. Welling, "Multiplicative normalizing flows for variational bayesian neural networks," in *Proceedings of the 34th International Conference on Machine Learning-Volume 70*. JMLR. org, 2017, pp. 2218–2227.
- [18] Y. Wen, P. Vicol, J. Ba, D. Tran, and R. Grosse, "Flipout: Efficient pseudo-independent weight perturbations on mini-batches," *International Conference on Learning Representations (ICLR)*, 2018.
- [19] B. Efron and R. Tibshirani, "Bootstrap methods for standard errors, confidence intervals, and other measures of statistical accuracy," *Statistical science*, pp. 54–75, 1986.
- [20] B. Lakshminarayanan, A. Pritzel, and C. Blundell, "Simple and scalable predictive uncertainty estimation using deep ensembles," in *Advances in Neural Information Processing Systems*, 2017, pp. 6402–6413.
- [21] P. Schulam and S. Saria, "Can you trust this prediction? auditing point-wise reliability after learning," in *The 22nd International Conference on Artificial Intelligence and Statistics*, 2019, pp. 1022–1031.
- [22] G. Wang, W. Li, T. Vercauteren, and S. Ourselin, "Automatic brain tumor segmentation based on cascaded convolutional neural networks with uncertainty estimation," *Frontiers in computational neuroscience*, vol. 13, p. 56, 2019.
- [23] T. Nair, D. Precup, D. L. Arnold, and T. Arbel, "Exploring uncertainty measures in deep networks for multiple sclerosis lesion detection and segmentation," *Medical Image Analysis*, p. 101557, 2019.
- [24] T. DeVries and G. W. Taylor, "Leveraging uncertainty estimates for predicting segmentation quality," *arXiv preprint arXiv:1807.00502*, 2018.
- [25] E. Hann, L. Biasioli, Q. Zhang, I. A. Popescu, K. Werys, E. Lukaschuk, V. Carapella, J. M. Paiva, N. Aung, J. J. Rayner *et al.*, "Quality control-driven image segmentation towards reliable automatic image analysis in large-scale cardiovascular magnetic resonance aortic cine imaging," in *International Conference on Medical Image Computing and Computer-Assisted Intervention*. Springer, 2019, pp. 750–758.
- [26] A. Jungo and M. Reyes, "Assessing reliability and challenges of uncertainty estimations for medical image segmentation," in *International Conference on Medical Image Computing and Computer-Assisted Intervention*. Springer, 2019, pp. 48–56.
- [27] A. Jungo, F. Balsiger, and M. Reyes, "Analyzing the quality and challenges of uncertainty estimations for brain tumor segmentation," *Frontiers in Neuroscience*, vol. 14, p. 282, 2020.
- [28] A. Mehrtash, W. M. Wells, C. M. Tempany, P. Abolmaesumi, and T. Kapur, "Confidence calibration and predictive uncertainty estimation for deep medical image segmentation," *IEEE Transactions on Medical Imaging*, 2020.
- [29] S. A. Kohl, B. Romera-Paredes, C. Meyer, J. De Fauw, J. R. Ledsam, K. H. Maier-Hein, S. Esлами, D. J. Rezende, and O. Ronneberger, "A probabilistic u-net for segmentation of ambiguous images," in *Advances in Neural Information Processing Systems*, 2018.
- [30] C. F. Baumgartner, K. C. Tezcan, K. Chaitanya, A. M. Hötker, U. J. Muehlemaier, K. Schawkat, A. S. Becker, O. Donati, and E. Konukoglu, "Phiseg: Capturing uncertainty in medical image segmentation," in *International Conference on Medical Image Computing and Computer-Assisted Intervention*. Springer, 2019, pp. 119–127.
- [31] M. Monteiro, L. L. Folgoc, D. C. de Castro, N. Pawłowski, B. Marques, K. Kamnitsas, M. van der Wilk, and B. Glocker, "Stochastic segmentation networks: Modelling spatially correlated aleatoric uncertainty," in *Advances in Neural Information Processing Systems*, 2020.
- [32] E. Puyol-Antón, B. Ruijsink, C. F. Baumgartner, P.-G. Masci, M. Sinclair, E. Konukoglu, R. Razavi, and A. P. King, "Automated quantification of myocardial tissue characteristics from native t1 mapping using neural networks with uncertainty-based quality-control," *Journal of Cardiovascular Magnetic Resonance*, vol. 22, no. 1, pp. 1–15, 2020.
- [33] D. J. MacKay, "Probable networks and plausible predictions—a review of practical bayesian methods for supervised neural networks," *Network: computation in neural systems*, vol. 6, no. 3, pp. 469–505, 1995.
- [34] M. D. Hoffman, D. M. Blei, C. Wang, and J. Paisley, "Stochastic variational inference," *The Journal of Machine Learning Research*, vol. 14, no. 1, pp. 1303–1347, 2013.
- [35] G. W. Brier *et al.*, "Verification of forecasts expressed in terms of probability," *Monthly weather review*, vol. 78, no. 1, pp. 1–3, 1950.
- [36] R. Camarasa, D. Bos, J. Hendrikse, P. Nederkoorn, M. E. Kooi, A. van der Lugt, M. de Bruijne *et al.*, "A quantitative comparison of epistemic uncertainty maps applied to multi-class segmentation," *Machine Learning for Biomedical Imaging*, vol. 1, no. UNSURE2020 special issue, pp. 1–10, 2021.
- [37] S. E. Petersen, P. M. Matthews, J. M. Francis, M. D. Robson, F. Zemrak, R. Boubertakh, A. A. Young, S. Hudson, P. Weale, S. Garratt *et al.*, "UK biobank's cardiovascular magnetic resonance protocol," *Journal of cardiovascular magnetic resonance*, vol. 18, no. 1, p. 8, 2015.
- [38] O. Ronneberger, P. Fischer, and T. Brox, "U-net: Convolutional networks for biomedical image segmentation," in *International Conference on Medical image computing and computer-assisted intervention*, N. Navab, J. Hornegger, W. M. Wells, and A. F. Frangi, Eds. Springer, 2015, pp. 234–241.
- [39] A. Kendall, V. Badrinarayanan, and R. Cipolla, "Bayesian segnet: Model uncertainty in deep convolutional encoder-decoder architectures for scene understanding," in *British Machine Vision Conference 2017, BMVC 2017*, 2017.
- [40] M. Fortunato, C. Blundell, and O. Vinyals, "Bayesian recurrent neural networks," *arXiv preprint arXiv:1704.02798*, 2017.
- [41] H. Gudbjartsson and S. Patz, "The rician distribution of noisy mri data," *Magnetic resonance in medicine*, vol. 34, no. 6, pp. 910–914, 1995.
- [42] B. Ruijsink, E. Puyol-Antón, I. Oksuz, M. Sinclair, W. Bai, J. A. Schnabel, R. Razavi, and A. P. King, "Fully automated, quality-controlled cardiac analysis from cmr: validation and large-scale application to characterize cardiac function," *JACC: Cardiovascular Imaging*, 2019.
- [43] G. Wang, W. Li, M. Aertsen, J. Depreest, S. Ourselin, and T. Vercauteren, "Aleatoric uncertainty estimation with test-time augmentation for medical image segmentation with convolutional neural networks," *Neurocomputing*, vol. 338, pp. 34–45, 2019.
- [44] A. Morcos, M. Raghu, and S. Bengio, "Insights on representational similarity in neural networks with canonical correlation," in *Advances in Neural Information Processing Systems*, 2018, pp. 5727–5736.
- [45] B. Ly, H. Cochet, and M. Sermesant, "Style data augmentation for robust segmentation of multi-modality cardiac mri," in *Statistical Atlases and Computational Modelling of the Heart*, 2019.
- [46] Y. Ganin, E. Ustinova, H. Ajakan, P. Germain, H. Larochelle, F. Laviolette, M. Marchand, and V. Lempitsky, "Domain-adversarial training of neural networks," *The Journal of Machine Learning Research*, vol. 17, no. 1, pp. 2096–2030, 2016.
- [47] X. Albà, K. Lekadir, M. Pereañez, P. Medrano-Gracia, A. A. Young, and A. F. Frangi, "Automatic initialization and quality control of large-scale cardiac mri segmentations," *Medical image analysis*, vol. 43, pp. 129–141, 2018.
- [48] R. Robinson, O. Oktay, W. Bai, V. V. Valindria, M. M. Sanghvi, N. Aung, J. M. Paiva, F. Zemrak, K. Fung, E. Lukaschuk, A. M. Lee, V. Carapella, Y. J. Kim, B. Kainz, S. K. Piechnik, S. Neubauer, S. E. Petersen, C. Page, D. Rueckert, and B. Glocker, "Real-time prediction of segmentation quality," in *International Conference on Medical Image Computing and Computer-Assisted Intervention*, A. F. Frangi, J. A. Schnabel, C. Davatzikos, C. Alberola-López, and G. Fichtinger, Eds. Springer, 2018, pp. 578–585.
- [49] J. Sander, B. D. de Vos, and I. Išgum, "Automatic segmentation with detection of local segmentation failures in cardiac mri," *Scientific Reports*, vol. 10, no. 1, pp. 1–19, 2020.
- [50] C. Gonzalez and A. Mukhopadhyay, "Self-supervised out-of-distribution detection for cardiac cmr segmentation," in *Medical Imaging with Deep Learning*. PMLR, 2021, pp. 205–218.
- [51] F. Galati and M. A. Zuluaga, "Efficient model monitoring for quality control in cardiac image segmentation," in *International Conference on Functional Imaging and Modeling of the Heart*. Springer, 2021, pp. 101–111.
- [52] R. Robinson, V. V. Valindria, W. Bai, O. Oktay, B. Kainz, H. Suzuki, M. M. Sanghvi, N. Aung, J. M. Paiva, F. Zemrak *et al.*, "Automated quality control in image segmentation: application to the uk biobank cardiovascular magnetic resonance imaging study," *Journal of Cardiovascular Magnetic Resonance*, vol. 21, no. 1, p. 18, 2019.

Supplementary Material to “Estimating Uncertainty in Neural Networks for Cardiac MRI Segmentation: A Benchmark Study”

Matthew Ng, Fumin Guo, Labonny Biswas, Steffen E. Petersen, Stefan K. Piechnik, Stefan Neubauer, Graham Wright

I. TRAINING DETAILS

For preprocessing, the input images were cropped to 160×160 pixels from the center of the original images. The cropped images were normalized by subtracting the mean and dividing by the variance of the entire training dataset. All the experiments were repeated 5 times (except for Deep Ensembles) and the resulting metrics were averaged. Data augmentation was performed, including random rotation (-60 to 60 degrees), translation (-60 to 60 pixels), and scaling (0.7 to 1.3 times). These models were trained using an Adam optimizer for 50 epochs. The initial learning rate was set to $1e-4$, which was decayed to $1e-5$ after 30 epochs.

All the experiments were performed on an Nvidia P100 GPU with 12GB of memory. SSN, MCD and BBB required approximately 20, 35 and 47 hours for training, respectively. For these methods, generating 50 prediction samples during testing required 1.5 seconds for each 2D image. The Deep Ensembles method consisted of 10 copies of the plain U-net and was trained in parallel separately. Each plain U-net required ~ 12 hours for training and ~ 0.1 seconds for prediction of a 2D image. Calculation of the predictive entropy, mutual information, Dice_{WS} , and ASSD_{WS} required approximately 0.05, 0.15, 0.15, and 0.4 seconds per image, respectively.

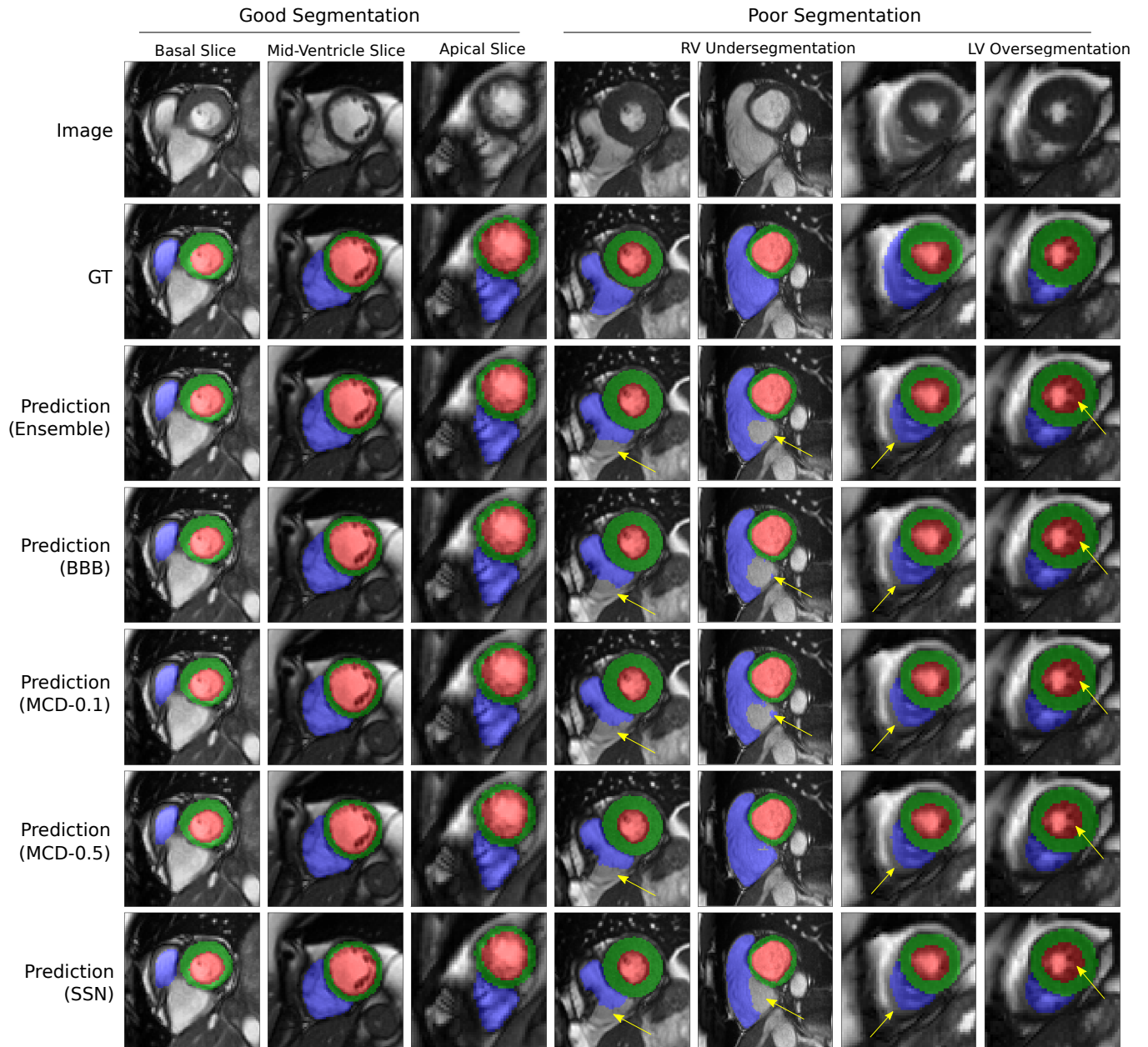


Fig. S1. Example segmentation results using the U-net with Deep Ensembles, BBB, MC Dropout (MCD), and SSN. Red = LV, green = Myo, blue = RV. Yellow arrows show area of inaccurate segmentation. Note that all methods have similar results. Reproduced by kind permission of UK Biobank ©.

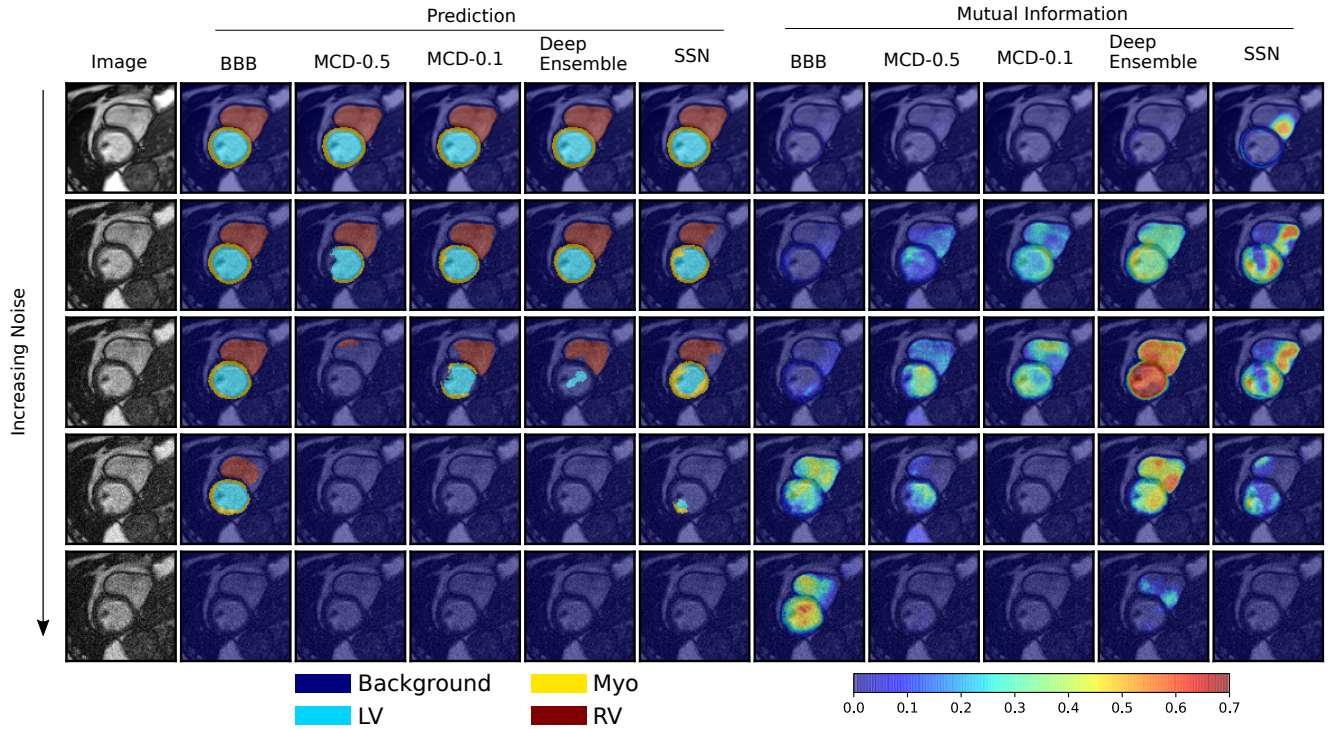


Fig. S2. Segmentation predictions and pixelwise uncertainty (mutual information) on images with increasing noise. Segmentation accuracy decreases while predictive uncertainty increases with more noise. Reproduced by kind permission of UK Biobank ©.

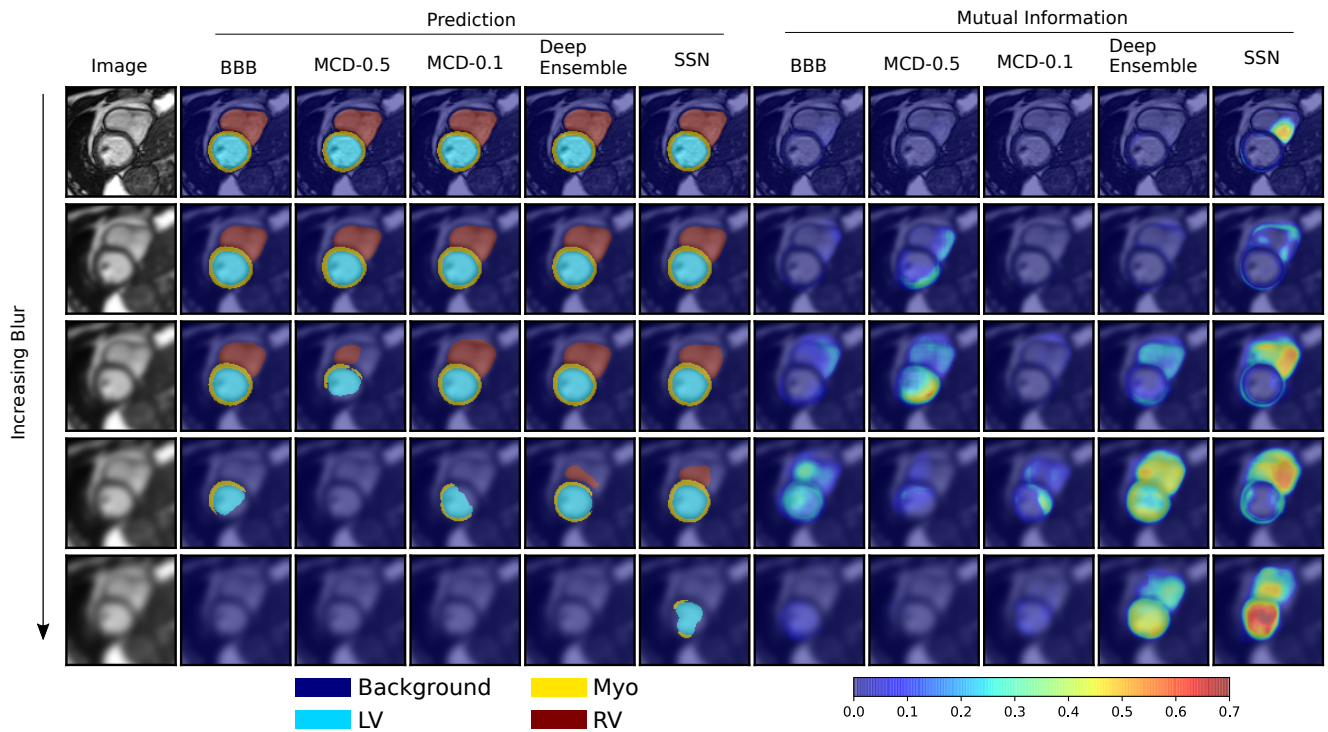


Fig. S3. Segmentation predictions and pixelwise uncertainty (mutual information) on images with increasing blur. Segmentation accuracy decreases while predictive uncertainty increases with more blurring. Reproduced by kind permission of UK Biobank ©.

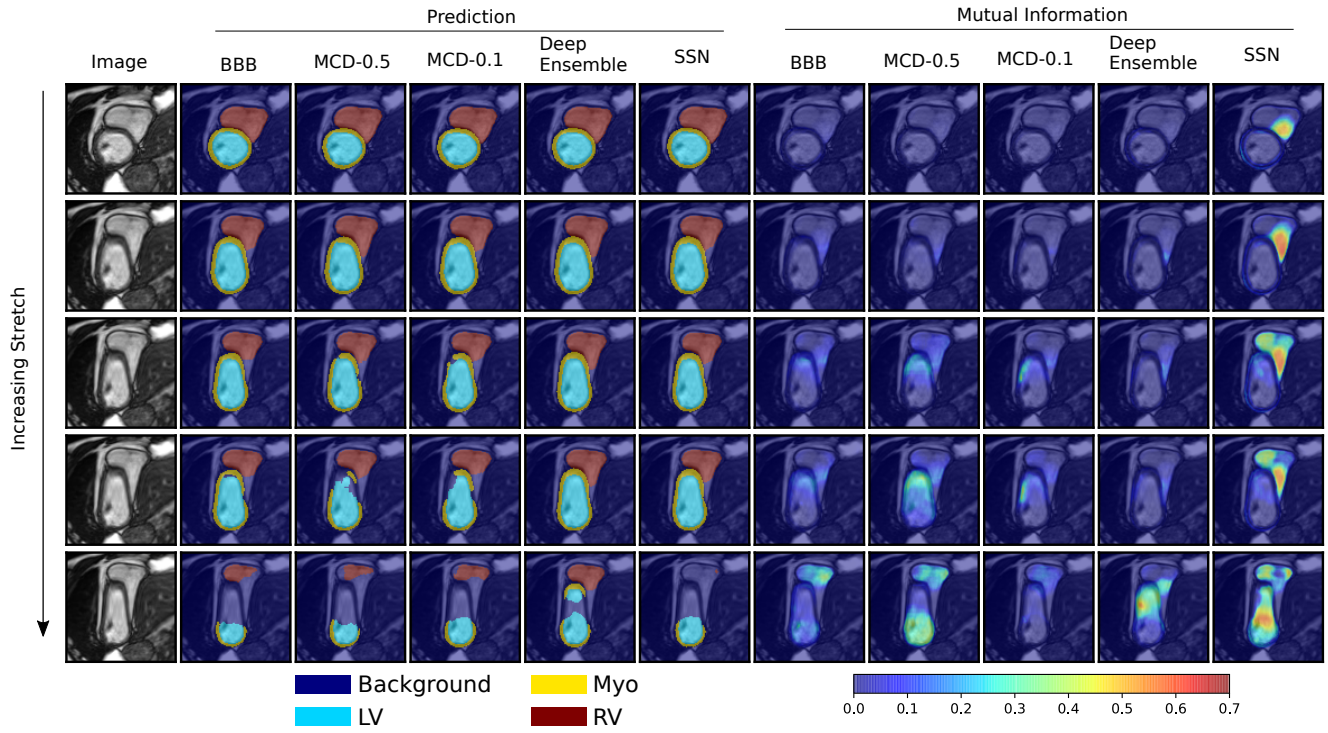


Fig. S4. Segmentation predictions and pixelwise uncertainty (mutual information) on images with increasing stretch. Segmentation accuracy decreases while predictive uncertainty increases with more stretching. Reproduced by kind permission of UK Biobank ©.

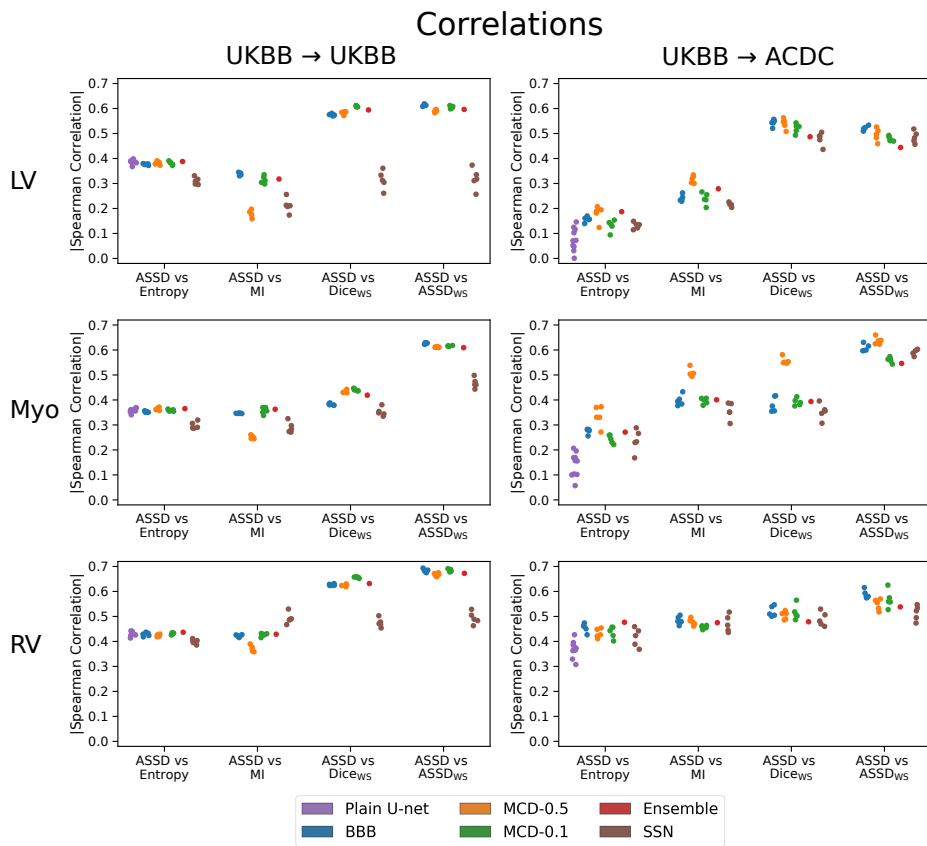


Fig. S5. Spearman correlations between segmentation accuracy (ASSD) and uncertainty measures (entropy, mutual information, Dice_{ws}, ASSD_{ws}) on the UKBB and ACDC datasets. Each point represents one run.

TABLE S1

SEGMENTATION ACCURACY ON IMAGES WITH INCREASING NOISE, BLURRING, AND STRETCHING DISTORTIONS. FORMAT: MEDIAN_{25-75TH} PERCENTILE

		Degree of Distortion				
		0	1	2	3	4
Pixelwise Accuracy	Plain U-net	.9960 _{.9944-.9973}	.9841 _{.9716-.9926}	.9749 _{.9599-.9887}	.9686 _{.9525-.9862}	.9648 _{.9464-.9854*}
	BBB	.9960 _{.9944-.9973}	.9929.9888-.9956	.9905.9833-.9947	.9862.9754-.9932	.9735.9593-.9883
	MCD-0.5	.9959 _{.9942-.9972}	.9807 _{.9673-.9913}	.9729 _{.9582-.9879}	.9678 _{.9514-.9859}	.9647 _{.9461-.9854*}
	MCD-0.1	.9960 _{.9944-.9973}	.9852 _{.9743-.9932}	.9767 _{.9627-.9889}	.9700 _{.9542-.9864}	.9649 _{.9467-.9854*}
	Ensemble	.9961.9945-.9973	.9873 _{.9717-.9941}	.9754 _{.9568-.9910}	.9679 _{.9495-.9871}	.9645 _{.9456-.9854*}
	SSN	.9960 _{.9943-.9972}	.9811 _{.9683-.9916}	.9725 _{.9574-.9878}	.9675 _{.9506-.9858}	.9648 _{.9460-.9854*}
Noise Dice LV	Plain U-net	.963 _{.932-.981}	.653 _{.194-.900}	.224 _{.010-.714}	.031 _{.000-.357}	.000 _{.000-.001*}
	BBB	.964 _{.934-.982}	.947.863-.976	.927.701-.972	.828.307-.961	.162.000-.753
	MCD-0.5	.963 _{.933-.981}	.657 _{.081-.944}	.235 _{.000-.762}	.000 _{.000-.452}	.000 _{.000-.000*}
	MCD-0.1	.963 _{.934-.982}	.714 _{.271-.951}	.356 _{.000-.753}	.024 _{.000-.529}	.000 _{.000-.000*}
	Ensemble	.965.936-.983	.873 _{.000-.970}	.000 _{.000-.937}	.000 _{.000-.000}	.000 _{.000-.000*}
	SSN	.963 _{.929-.981}	.501 _{.157-.911}	.171 _{.000-.643}	.041 _{.000-.247}	.000 _{.000-.000*}
ASSD LV	Plain U-net	0.77 _{0.47-1.15}	8.51 _{1.79-19.14}	19.24 _{8.03-31.70}	28.37 _{14.20-39.34}	34.85 _{19.52-45.93*}
	BBB	0.76 _{0.45-1.14}	1.070.61-2.05	1.420.69-4.40	2.710.88-13.65	19.444.20-33.37
	MCD-0.5	0.78 _{0.47-1.16}	8.99 _{1.23-21.06}	18.19 _{5.02-31.04}	27.22 _{12.21-37.95}	34.63 _{19.59-45.52*}
	MCD-0.1	0.77 _{0.46-1.15}	8.11 _{1.10-15.77}	15.23 _{7.73-28.31}	25.11 _{11.62-37.28}	34.32 _{19.19-45.60*}
	Ensemble	0.740.43-1.12	2.30 _{0.73-22.35}	20.49 _{1.36-38.93}	32.75 _{10.46-45.01}	35.45 _{19.79-47.01*}
	SSN	0.78 _{0.47-1.17}	11.09 _{1.81-22.62}	21.95 _{7.17-31.65}	28.74 _{15.31-38.76}	34.49 _{19.82-45.70*}
Gaussian Blur Pixelwise Accuracy	Plain U-net	.9960 _{.9944-.9973}	.9910 _{.9868-.9942}	.9842 _{.9759-.9913}	.9732 _{.9609-.9878}	.9664 _{.9494-.9856[†]}
	BBB	.9960 _{.9944-.9973}	.9922 _{.9889-.9948}	.9864 _{.9779-.9921}	.9726 _{.9583-.9876}	.9656 _{.9465-.9855[†]}
	MCD-0.5	.9959 _{.9942-.9972}	.9894 _{.9829-.9936}	.9779 _{.9637-.9904}	.9676 _{.9491-.9869}	.9647 _{.9456-.9854[†]}
	MCD-0.1	.9960 _{.9944-.9973}	.9915 _{.9873-.9945}	.9847 _{.9747-.9917}	.9713 _{.9563-.9875}	.9652 _{.9461-.9854[†]}
	Ensemble	.9961.9945-.9973	.9923.9887-.9950	.9871.9780-.9926	.9730 _{.9580-.9881}	.9655 _{.9460-.9855[†]}
	SSN	.9960 _{.9943-.9972}	.9907 _{.9857-.9943}	.9839 _{.9743-.9920}	.9748.9610-.9893	.9682.9496-.9867
Gaussian Blur Dice LV	Plain U-net	.963 _{.932-.981}	.910 _{.818-.959}	.833 _{.616-.931}	.535 _{.127-.780}	.093 _{.000-.349[†]}
	BBB	.964 _{.934-.982}	.936 _{.869-.967}	.883 _{.659-.949}	.466 _{.000-.807}	.000 _{.000-.180[†]}
	MCD-0.5	.963 _{.933-.981}	.922 _{.829-.963}	.726 _{.191-.915}	.066 _{.000-.491}	.000 _{.000-.000[†]}
	MCD-0.1	.964 _{.934-.982}	.928 _{.838-.964}	.864 _{.549-.952}	.356 _{.000-.790}	.000 _{.000-.129[†]}
	Ensemble	.965.936-.983	.940.876-.970	.914.775-.964	.688 _{.000-.928}	.000 _{.000-.000[†]}
	SSN	.963 _{.929-.981}	.921 _{.831-.960}	.884 _{.744-.946}	.726.192-.885	.146.000-.639
ASSD LV	Plain U-net	0.77 _{0.47-1.15}	1.50 _{0.96-2.86}	2.91 _{1.37-9.46}	12.59 _{4.59-23.71}	27.88 _{13.87-39.61[†]}
	BBB	0.76 _{0.45-1.14}	1.26 _{0.80-2.01}	2.06 _{1.13-5.93}	13.61 _{3.03-27.63}	32.37 _{16.40-44.20[†]}
	MCD-0.5	0.78 _{0.47-1.16}	1.43 _{0.88-2.48}	4.49 _{1.48-21.05}	27.73 _{9.68-40.34}	35.11 _{19.08-46.65[†]}
	MCD-0.1	0.76 _{0.46-1.15}	1.35 _{0.86-2.31}	2.22 _{1.12-9.11}	14.70 _{3.25-31.19}	33.21 _{16.91-45.17[†]}
	Ensemble	0.740.43-1.12	1.220.74-1.94	1.580.89-3.34	4.99 _{1.47-32.70}	34.17 _{11.37-46.57[†]}
	SSN	0.78 _{0.47-1.17}	1.41 _{0.92-2.37}	1.99 _{1.18-3.96}	4.491.99-16.66	21.575.50-37.39
Pixelwise Accuracy	Plain U-net	.9960 _{.9944-.9973}	.9921 _{.9896-.9940}	.9879 _{.9820-.9925}	.9841 _{.9767-.9912}	.9729 _{.9645-.9852[§]}
	BBB	.9960 _{.9944-.9973}	.9918 _{.9889-.9939}	.9849 _{.9767-.9916}	.9793 _{.9698-.9895}	.9684 _{.9577-.9834[§]}
	MCD-0.5	.9959 _{.9942-.9972}	.9924 _{.9897-.9942}	.9887 _{.9816-.9928}	.9846 _{.9757-.9913}	.9720 _{.9628-.9846[§]}
	MCD-0.1	.9960 _{.9944-.9973}	.9922 _{.9897-.9941}	.9881 _{.9817-.9926}	.9837 _{.9761-.9911}	.9722 _{.9638-.9845[§]}
	Ensemble	.9961.9945-.9973	.9925.9902-.9944	.9894.9826-.9933	.9857.9768-.9923	.9730.9638-.9864[§]
	SSN	.9960 _{.9943-.9972}	.9919 _{.9889-.9940}	.9860 _{.9794-.9920}	.9813 _{.9740-.9902}	.9706 _{.9626-.9834[§]}
Stretch Dice LV	Plain U-net	.963 _{.932-.981}	.945 _{.895-.969}	.902 _{.762-.963}	.861 _{.697-.955}	.648 _{.402-.838[§]}
	BBB	.964 _{.934-.982}	.946 _{.886-.970}	.856 _{.644-.960}	.778 _{.541-.944}	.530 _{.210-.754[§]}
	MCD-0.5	.963 _{.933-.981}	.949 _{.900-.971}	.916 _{.739-.967}	.862 _{.654-.961}	.626 _{.358-.809[§]}
	MCD-0.1	.964 _{.934-.982}	.948 _{.898-.970}	.907 _{.742-.965}	.853 _{.658-.958}	.615 _{.343-.816[§]}
	Ensemble	.965.936-.983	.952.910-.972	.933.799-.969	.892.722-.967	.672.442-.859[§]
	SSN	.963 _{.929-.981}	.944 _{.876-.969}	.867 _{.670-.961}	.805 _{.598-.946}	.568 _{.295-.780[§]}
ASSD LV	Plain U-net	0.77 _{0.47-1.15}	1.11 _{0.79-1.60}	1.58 _{0.90-3.53}	2.25 _{1.04-5.10}	6.81 _{2.63-14.20[§]}
	BBB	0.76 _{0.45-1.14}	1.11 _{0.78-1.70}	2.20 _{0.95-5.68}	3.65 _{1.18-8.26}	9.84 _{4.27-21.04[§]}
	MCD-0.5	0.78 _{0.47-1.16}	1.05 _{0.76-1.51}	1.38 _{0.81-3.70}	2.10 _{0.92-5.72}	7.50 _{2.99-12.36[§]}
	MCD-0.1	0.76 _{0.46-1.15}	1.08 _{0.77-1.56}	1.51 _{0.86-3.83}	2.35 _{1.00-5.76}	7.73 _{3.15-16.29[§]}
	Ensemble	0.740.43-1.12	1.020.72-1.46	1.210.75-2.91	1.660.82-4.62	6.361.89-11.22
	SSN	0.78 _{0.47-1.17}	1.11 _{0.80-1.72}	2.04 _{0.93-5.19}	3.12 _{1.15-7.22}	8.78 _{3.96-19.33[§]}

* statistically different compared to BBB (Wilcoxon signed-rank test, $p < 0.05$).[†] statistically different compared to SSN (Wilcoxon signed-rank test, $p < 0.05$).[§] statistically different compared to Ensemble (Wilcoxon signed-rank test, $p < 0.05$).

TABLE S2
PROBABILITY CALIBRATION ON IMAGES WITH INCREASING NOISE, BLURRING, OR STRETCHING DISTORTIONS. FORMAT:
MEDIAN_{25-75TH PERCENTILE}

		Degree of Distortion					
		0	1	2	3	4	
Noise	NLL ($\times 10^{-2}$)	Plain U-net	0.94 _{0.66-1.32}	8.53 _{2.68-19.45}	20.37 _{7.63-38.49}	32.64 _{13.47-54.87}	47.85 _{19.72-73.98} *
		BBB	0.95 _{0.67-1.31}	1.73 _{1.10-2.70}	2.35 _{1.33-4.08}	3.54 _{1.79-6.58}	8.52 _{3.81-15.41}
		MCD-0.5	0.97 _{0.69-1.35}	6.16 _{2.70-12.12}	11.13 _{4.86-20.18}	17.15 _{7.76-29.21}	29.91 _{13.40-45.40} *
		MCD-0.1	0.94 _{0.67-1.32}	4.90 _{1.94-11.47}	12.67 _{4.72-23.80}	22.00 _{9.79-37.35}	38.16 _{16.56-59.05} *
		Ensemble	0.92 _{0.65-1.28}	3.54 _{1.66-7.51}	7.40 _{2.98-15.80}	13.87 _{5.29-29.21}	32.59 _{12.42-55.13} *
		SSN	0.97 _{0.69-1.39}	6.71 _{2.74-15.81}	16.30 _{5.63-32.33}	28.49 _{11.37-48.30}	46.80 _{20.20-71.57} *
	Brier Score ($\times 10^{-3}$)	Plain U-net	1.43 _{0.99-2.01}	6.64 _{2.92-12.52}	11.38 _{5.03-18.82}	14.97 _{6.60-22.88}	17.52 _{7.27-26.58} *
		BBB	1.43 _{1.00-2.00}	2.55 _{1.62-4.00}	3.44 _{1.94-5.93}	5.04 _{2.51-9.03}	10.45 _{4.72-16.48}
		MCD-0.5	1.47 _{1.02-2.06}	7.53 _{3.42-13.17}	11.28 _{5.11-17.95}	14.38 _{6.43-21.71}	17.13 _{7.24-25.99} *
		MCD-0.1	1.43 _{0.99-2.01}	5.77 _{2.57-10.48}	9.91 _{4.62-16.20}	13.46 _{6.28-21.03}	17.14 _{7.24-26.03} *
		Ensemble	1.40 _{0.96-1.96}	4.99 _{2.30-10.45}	9.57 _{3.83-17.19}	13.90 _{5.78-21.92}	17.37 _{7.26-26.34} *
		SSN	1.46 _{1.02-2.10}	7.30 _{3.35-12.74}	11.58 _{5.16-18.69}	14.89 _{6.66-22.89}	17.38 _{7.26-26.61} *
Gaussian Blur	NLL ($\times 10^{-2}$)	Plain U-net	0.94 _{0.66-1.32}	2.26 _{1.54-3.46}	4.77 _{2.60-8.96}	12.30 _{5.18-22.95}	24.51 _{9.26-41.24} †
		BBB	0.95 _{0.67-1.31}	1.96 _{1.41-2.73}	3.47 _{2.21-5.28}	8.22 _{4.38-13.31}	17.92 _{8.53-28.82} †
		MCD-0.5	0.97 _{0.69-1.35}	2.71 _{1.76-3.99}	5.59 _{2.89-9.69}	12.59 _{5.22-22.19}	21.42 _{8.84-35.15} †
		MCD-0.1	0.94 _{0.67-1.32}	2.10 _{1.47-3.17}	4.11 _{2.39-7.36}	11.28 _{4.96-19.86}	23.53 _{9.88-37.88} †
		Ensemble	0.92 _{0.65-1.28}	1.99 _{1.41-2.79}	3.37 _{2.17-5.03}	6.72 _{3.87-10.38}	13.36 _{6.71-21.80} ¶
		SSN	0.97 _{0.70-1.39}	2.28 _{1.53-3.45}	3.93 _{2.14-6.49}	7.12 _{3.19-13.22}	12.94 _{4.85-25.22}
	Brier Score ($\times 10^{-3}$)	Plain U-net	1.43 _{0.99-2.01}	3.27 _{2.19-4.85}	5.99 _{3.32-9.63}	11.43 _{5.18-17.25}	15.81 _{6.77-23.88} †
		BBB	1.43 _{1.00-2.00}	2.86 _{2.01-4.02}	4.99 _{3.02-7.78}	10.59 _{5.08-16.29}	15.73 _{6.93-24.06} †
		MCD-0.5	1.47 _{1.02-2.06}	3.92 _{2.46-5.98}	7.98 _{3.72-13.57}	13.96 _{5.62-21.96}	16.85 _{7.11-26.23} †
		MCD-0.1	1.43 _{0.99-2.01}	3.07 _{2.08-4.63}	5.66 _{3.17-9.59}	11.97 _{5.26-18.55}	16.50 _{7.04-25.56} †
		Ensemble	1.40 _{0.96-1.96}	2.88 _{1.99-4.12}	4.85 _{2.95-7.55}	9.80 _{4.85-14.91}	15.20 _{6.65-22.65} †
		SSN	1.46 _{1.03-2.11}	3.38 _{2.19-5.15}	5.73 _{2.96-9.23}	9.47 _{4.00-15.24}	13.32 _{5.39-21.28}
Stretch	NLL ($\times 10^{-2}$)	Plain U-net	0.94 _{0.66-1.32}	1.96 _{1.47-2.66}	3.34 _{1.95-5.73}	4.88 _{2.37-8.67}	13.35 _{6.05-19.84} §
		BBB	0.95 _{0.67-1.31}	2.03 _{1.53-2.72}	3.74 _{2.19-5.97}	5.37 _{2.82-8.83}	12.42 _{6.07-18.46} §
		MCD-0.5	0.97 _{0.69-1.35}	1.89 _{1.42-2.53}	2.90 _{1.90-4.72}	4.01 _{2.35-6.91}	9.97 _{5.07-14.89} §
		MCD-0.1	0.94 _{0.67-1.32}	1.94 _{1.45-2.58}	3.09 _{1.92-5.02}	4.40 _{2.38-7.53}	11.38 _{5.57-16.73} §
		Ensemble	0.92 _{0.65-1.28}	1.84 _{1.39-2.40}	2.73 _{1.76-4.11}	3.65 _{2.09-5.79}	8.66 _{4.32-12.76}
		SSN	0.97 _{0.69-1.39}	2.05 _{1.52-2.78}	3.66 _{2.10-5.58}	5.20 _{2.65-8.06}	12.93 _{6.76-18.13} §
	Brier Score ($\times 10^{-3}$)	Plain U-net	1.43 _{0.99-2.01}	2.86 _{2.17-3.76}	4.48 _{2.75-6.92}	6.10 _{3.26-9.35}	11.58 _{6.20-15.56} §
		BBB	1.43 _{1.00-2.00}	2.96 _{2.23-3.97}	5.41 _{3.09-8.38}	7.58 _{3.90-11.45}	13.12 _{7.03-17.91} §
		MCD-0.5	1.47 _{1.02-2.06}	2.77 _{2.10-3.69}	4.13 _{2.70-6.59}	5.62 _{3.29-9.01}	11.24 _{6.25-15.14} §
		MCD-0.1	1.43 _{0.99-2.01}	2.82 _{2.15-3.71}	4.34 _{2.74-6.71}	5.97 _{3.31-9.18}	11.52 _{6.40-15.33} §
		Ensemble	1.40 _{0.96-1.96}	2.70 _{2.05-3.50}	3.90 _{2.52-6.08}	5.26 _{2.94-8.34}	10.67 _{5.49-14.49}
		SSN	1.46 _{1.02-2.10}	2.97 _{2.21-4.02}	5.09 _{2.97-7.44}	6.89 _{3.66-9.73}	12.11 _{6.92-15.61} §

* statistically different compared to BBB (Wilcoxon signed-rank test, $p < 0.05$).

† statistically different compared to SSN (Wilcoxon signed-rank test, $p < 0.05$).

¶ not statistically different compared to SSN (Wilcoxon signed-rank test, $p > 0.05$).

§ statistically different compared to Ensemble (Wilcoxon signed-rank test, $p < 0.05$).

TABLE S3
 PREDICTIVE UNCERTAINTY MEASURES ON IMAGES WITH INCREASING NOISE, BLURRING, OR STRETCHING DISTORTIONS. FOR EACH ROW, THE BOLDDED ITEM INDICATES THE DEGREE OF DISTORTION WITH THE HIGHEST UNCERTAINTY. FORMAT: MEDIAN_{25-75TH PERCENTILE}

		Degree of Distortion					
		0	1	2	3	4	
Noise	Pred Entropy ($\times 10^{-2}$)	Plain U-net	1.03 _{0.76-1.32}	1.10_{0.29-1.72}	0.47 _{0.10-1.32}	0.13 _{0.04-0.60}	0.02 _{0.01-0.05}
		BBB	1.11 _{0.82-1.43}	1.66 _{0.99-2.34}	1.85 _{0.93-2.67}	1.95_{0.72-2.91}	1.23 _{0.33-2.65}
		MCD-0.5	1.10 _{0.82-1.43}	2.13_{1.12-3.09}	1.65 _{0.90-2.77}	1.11 _{0.69-1.96}	0.51 _{0.35-0.75}
		MCD-0.1	1.06 _{0.79-1.36}	1.50_{0.49-2.18}	1.00 _{0.22-1.95}	0.40 _{0.11-1.31}	0.08 _{0.05-0.22}
		Ensemble	1.05 _{0.78-1.35}	1.74_{0.42-3.05}	0.88 _{0.16-2.79}	0.22 _{0.05-1.35}	0.03 _{0.01-0.07}
		SSN	1.13 _{0.87-1.52}	1.66_{0.71-2.70}	0.97 _{0.41-2.04}	0.48 _{0.21-1.04}	0.08 _{0.02-0.22}
	MI ($\times 10^{-3}$)	BBB	0.32 _{0.24-0.43}	1.26 _{0.65-2.46}	2.19 _{0.91-4.79}	3.54 _{1.12-7.38}	3.85_{0.75-9.38}
		MCD-0.5	0.16 _{0.11-0.29}	4.32_{2.18-6.96}	4.10 _{2.02-7.16}	2.82 _{1.56-5.75}	1.23 _{0.79-2.00}
		MCD-0.1	0.09 _{0.06-0.13}	1.68_{0.44-3.54}	1.65 _{0.26-3.83}	0.74 _{0.14-2.92}	0.13 _{0.06-0.51}
		Ensemble	0.22 _{0.16-0.34}	5.42_{1.06-14.00}	3.61 _{0.47-14.15}	0.82 _{0.14-7.07}	0.07 _{0.03-0.24}
		SSN	2.90 _{2.11-5.22}	8.95_{3.91-14.29}	5.49 _{2.23-11.45}	2.63 _{1.08-5.99}	0.38 _{0.09-1.17}
	Dicews LV	BBB	.990 _{.984-.994}	.976 _{.920-.990}	.948 _{.804-.984}	.876 _{.699-.972}	.820_{.656-.980}
		MCD-0.5	.994 _{.990-.997}	.856 _{.714-.964}	.835_{.689-.956}	.892 _{.723-.976}	.984 _{.936-.996}
		MCD-0.1	.995 _{.992-.997}	.931 _{.836-.990}	.920_{.813-.996}	.968 _{.838-1.00}	1.00 _{.988-1.00}
		Ensemble	.993 _{.987-.996}	.862_{.672-.987}	.885 _{.670-1.00}	1.00 _{.800-1.00}	1.00 _{1.00-1.00}
		SSN	.971 _{.935-.984}	.798_{.678-.902}	.842 _{.701-.942}	.920 _{.805-.980}	.990 _{.962-.998}
	ASSD _{WS} LV	BBB	0.21 _{0.17-0.27}	0.45 _{0.25-1.07}	0.86 _{0.32-2.65}	1.90 _{0.47-4.67}	2.96_{0.17-6.60}
		MCD-0.5	0.12 _{0.08-0.16}	2.51 _{0.62-5.04}	2.94_{0.57-5.92}	1.89 _{0.23-5.40}	0.17 _{0.00-1.07}
		MCD-0.1	0.10 _{0.07-0.14}	1.02 _{0.17-2.34}	1.16_{0.00-2.75}	0.41 _{0.00-2.33}	0.00 _{0.00-0.10}
		Ensemble	0.16 _{0.11-0.22}	3.34_{0.26-7.43}	2.48 _{0.00-8.84}	0.00 _{0.00-4.48}	0.00 _{0.00-0.00}
SSN		0.55 _{0.41-0.85}	4.15_{1.80-7.28}	3.44 _{1.16-6.77}	1.59 _{0.55-4.36}	0.21 _{0.01-0.79}	
Gaussian Blur	Pred Entropy ($\times 10^{-2}$)	Plain U-net	1.03 _{0.76-1.32}	2.01_{1.27-2.58}	1.98 _{0.94-2.82}	1.34 _{0.33-2.29}	0.44 _{0.16-1.11}
		BBB	1.11 _{0.82-1.43}	2.28 _{1.43-3.02}	2.47_{1.22-3.69}	1.71 _{0.47-3.07}	0.52 _{0.16-1.36}
		MCD-0.5	1.10 _{0.82-1.43}	2.52_{1.44-3.62}	2.13 _{0.84-3.58}	1.04 _{0.33-2.16}	0.33 _{0.20-0.65}
		MCD-0.1	1.06 _{0.79-1.37}	2.09 _{1.35-2.69}	2.11_{0.99-3.12}	1.29 _{0.30-2.40}	0.30 _{0.13-0.75}
		Ensemble	1.05 _{0.78-1.35}	2.31 _{1.42-3.11}	2.55_{1.17-3.99}	1.90 _{0.44-3.75}	0.67 _{0.21-1.87}
		SSN	1.13 _{0.87-1.53}	2.44 _{1.67-3.23}	2.50_{1.57-3.52}	2.14 _{1.13-3.28}	1.43 _{0.73-2.32}
	MI ($\times 10^{-3}$)	BBB	0.32 _{0.24-0.43}	1.64 _{0.83-2.90}	3.63 _{1.39-6.82}	3.71_{1.07-8.27}	1.55 _{0.36-4.11}
		MCD-0.5	0.16 _{0.11-0.29}	3.10 _{1.34-5.50}	4.03_{1.20-8.87}	2.39 _{0.57-5.93}	0.64 _{0.33-1.64}
		MCD-0.1	0.09 _{0.06-0.13}	0.81 _{0.37-1.66}	1.43_{0.51-2.89}	1.09 _{0.26-2.68}	0.28 _{0.09-0.81}
		Ensemble	0.22 _{0.16-0.34}	2.55 _{1.09-5.37}	5.46_{1.62-11.59}	5.13 _{0.92-14.59}	2.01 _{0.41-7.38}
		SSN	2.90 _{2.10-5.21}	9.74 _{6.29-15.59}	11.89_{7.25-17.71}	10.90 _{5.85-17.76}	7.92 _{3.84-12.95}
	Dicews LV	BBB	.990 _{.984-.994}	.979 _{.958-.986}	.944 _{.840-.974}	.816_{.688-.988}	.964 _{.804-1.00}
		MCD-0.5	.994 _{.990-.997}	.972 _{.891-.986}	.878_{.708-.980}	.911 _{.732-1.00}	1.00 _{.972-1.00}
		MCD-0.1	.995 _{.992-.997}	.988 _{.968-.993}	.976 _{.898-.990}	.921_{.788-1.00}	1.00 _{.956-1.00}
		Ensemble	.993 _{.987-.996}	.977 _{.928-.987}	.945 _{.822-.979}	.829_{.610-1.00}	.900 _{.700-1.00}
		SSN	.971 _{.936-.984}	.921 _{.768-.952}	.855 _{.736-.909}	.765_{.635-.876}	.772 _{.604-.938}
	ASSD _{WS} LV	BBB	0.21 _{0.17-0.27}	0.40 _{0.31-0.73}	1.06 _{0.44-3.03}	3.40_{0.19-6.34}	0.71 _{0.00-4.36}
		MCD-0.5	0.12 _{0.08-0.16}	0.54 _{0.26-1.99}	2.35_{0.28-6.10}	1.79 _{0.00-5.77}	0.00 _{0.00-0.62}
		MCD-0.1	0.10 _{0.07-0.14}	0.22 _{0.16-0.47}	0.43 _{0.19-1.45}	1.10_{0.00-2.99}	0.00 _{0.00-0.62}
		Ensemble	0.16 _{0.11-0.22}	0.43 _{0.30-0.90}	0.92 _{0.40-4.67}	3.79_{0.00-9.50}	0.78 _{0.00-6.59}
SSN		0.56 _{0.41-0.86}	1.25 _{0.96-4.28}	2.84 _{1.59-6.02}	4.98_{2.39-8.40}	4.90 _{1.53-8.23}	
Stretch	Pred Entropy ($\times 10^{-2}$)	Plain U-net	1.03 _{0.76-1.32}	1.68 _{1.30-2.04}	1.87 _{1.04-2.30}	1.95_{0.95-2.46}	1.30 _{0.60-2.11}
		BBB	1.11 _{0.82-1.43}	1.98 _{1.51-2.44}	2.39_{1.21-3.06}	2.38 _{1.08-3.26}	1.46 _{0.70-2.39}
		MCD-0.5	1.10 _{0.82-1.43}	1.76 _{1.40-2.25}	2.19 _{1.30-2.82}	2.39_{1.19-3.16}	1.72 _{0.77-2.91}
		MCD-0.1	1.06 _{0.79-1.37}	1.70 _{1.34-2.10}	2.01 _{1.14-2.55}	2.14_{1.05-2.80}	1.50 _{0.65-2.49}
		Ensemble	1.05 _{0.78-1.35}	1.80 _{1.40-2.24}	2.17 _{1.25-2.86}	2.33_{1.15-3.18}	1.71 _{0.75-2.95}
		SSN	1.13 _{0.87-1.52}	2.00 _{1.59-2.52}	2.38 _{1.53-2.95}	2.47_{1.45-3.14}	1.70 _{0.91-2.66}
	MI ($\times 10^{-3}$)	BBB	0.32 _{0.24-0.43}	1.03 _{0.60-1.81}	2.48 _{1.02-4.88}	2.92_{1.10-5.68}	2.25 _{0.80-4.71}
		MCD-0.5	0.16 _{0.11-0.29}	0.87 _{0.42-1.76}	2.57 _{1.02-5.18}	3.49 _{1.35-6.94}	3.64_{1.14-7.55}
		MCD-0.1	0.09 _{0.06-0.13}	0.36 _{0.19-0.72}	1.10 _{0.40-2.21}	1.44 _{0.50-2.85}	1.44_{0.43-3.20}
		Ensemble	0.23 _{0.16-0.34}	0.91 _{0.50-1.67}	2.50 _{1.01-5.22}	3.26 _{1.24-6.78}	3.62_{1.19-7.93}
		SSN	2.89 _{2.11-5.23}	6.87 _{4.54-10.97}	9.93 _{6.70-13.08}	10.72_{7.12-14.13}	8.53 _{4.84-12.87}
	Dicews LV	BBB	.990 _{.984-.994}	.983 _{.956-.993}	.937 _{.834-.982}	.922 _{.802-.970}	.865_{.696-.950}
		MCD-0.5	.994 _{.990-.997}	.989 _{.965-.996}	.951 _{.864-.991}	.928 _{.838-.980}	.870_{.724-.937}
		MCD-0.1	.995 _{.992-.997}	.992 _{.979-.997}	.971 _{.919-.995}	.960 _{.895-.989}	.918_{.814-.968}
		Ensemble	.993 _{.987-.996}	.987 _{.968-.995}	.960 _{.900-.993}	.947 _{.877-.990}	.899_{.737-.958}
		SSN	.971 _{.936-.984}	.930 _{.803-.974}	.828 _{.688-.925}	.808 _{.677-.909}	.741_{.619-.851}
	ASSD _{WS} LV	BBB	0.21 _{0.17-0.27}	0.33 _{0.19-0.63}	0.93 _{0.34-2.12}	1.18 _{0.47-2.53}	1.80_{0.68-3.36}
		MCD-0.5	0.12 _{0.08-0.16}	0.20 _{0.10-0.50}	0.74 _{0.18-1.81}	1.12 _{0.33-2.21}	2.00_{0.90-3.34}
		MCD-0.1	0.10 _{0.07-0.14}	0.16 _{0.09-0.31}	0.45 _{0.13-1.03}	0.64 _{0.19-1.30}	1.11_{0.47-1.95}
		Ensemble	0.16 _{0.11-0.22}	0.28 _{0.16-0.48}	0.62 _{0.20-1.37}	0.81 _{0.25-1.84}	1.58_{0.56-3.92}
SSN		0.56 _{0.41-0.85}	1.09 _{0.55-3.31}	2.93 _{1.16-6.01}	3.28 _{1.47-6.33}	4.45_{2.44-7.02}	

TABLE S4
SEGMENTATION ACCURACY AND PROBABILITY CALIBRATION METRICS ON THE ACDC AND UKBB DATASETS USING MODELS TRAINED WITH UKBB DATASET. FORMAT: MEDIAN_{25-75TH PERCENTILE}

	Pixelwise Accuracy ↑	Dice ↑			ASSD (mm) ↓			NLL ↓ ($\times 10^{-2}$)	BS ↓ ($\times 10^{-3}$)
		LV	Myo	RV	LV	Myo	RV		
UKBB → UKBB									
Plain U-net	.9960 _{.9944-0.9973}	.963 _{.932-0.981}	.899 _{.847-0.929}	.929 _{.850-0.964}	0.77 _{0.46-1.15}	0.82 _{0.58-1.12}	1.12 _{0.74-1.79}	0.94 _{0.66-1.32}	1.43 _{0.99-2.01}
BBB	.9960 _{.9944-0.9973}	.964 _{.934-0.982}	.899 _{.849-0.930}	.931 _{.853-0.966}	0.76 _{0.45-1.14}	0.82 _{0.57-1.12}	1.10 _{0.72-1.76}	0.95 _{0.67-1.31}	1.43 _{1.00-2.00}
MCD-0.1	.9960 _{.9944-0.9973}	.964 _{.934-0.982}	.899 _{.847-0.930}	.931 _{.850-0.965}	0.77 _{0.46-1.15}	0.82 _{0.58-1.12}	1.11 _{0.73-1.77}	0.94 _{0.67-1.31}	1.43 _{0.99-2.01}
MCD-0.5	.9959 _{.9942-0.9972}	.963 _{.933-0.981}	.896 _{.845-0.927}	.929 _{.847-0.964}	0.78 _{0.47-1.16}	0.84 _{0.60-1.15}	1.13 _{0.74-1.82}	0.97 _{0.69-1.35}	1.47 _{1.02-2.06}
Ensemble	.9961_{.9945-0.9974}	.965_{.936-0.983}	.902_{.852-0.933}	.935_{.863-0.967}	0.74_{0.43-1.13}	0.80_{0.55-1.10}	1.07_{0.69-1.71}	0.92_{0.65-1.28}	1.40_{0.97-1.96}
SSN	.9960 _{.9943-0.9973}	.963 _{.929-0.981}	.896 _{.839-0.928}	.921 _{.820-0.961}	0.78 _{0.47-1.17}	0.84 _{0.59-1.16}	1.19 _{0.79-2.02}	0.97 _{0.69-1.39}	1.46 _{1.02-2.10}
UKBB → ACDC									
Plain U-net	.9880 _{.9790-0.9923}	.927 _{.781-0.960}	.833 _{.728-0.871}	.870 _{.600-0.938}	1.40 _{1.00-2.94}	1.40 _{1.10-2.64}	1.86 _{1.09-5.96}	3.12 _{1.87-7.17}	4.39 _{2.77-8.05}
BBB	.9888 _{.9814-0.9927}	.938 _{.856-0.964}	.843 _{.769-0.876}	.884 _{.615-0.943}	1.27 _{0.93-2.12}	1.32 _{1.05-1.97}	1.64 _{1.03-4.84}	2.76 _{1.76-4.85}	4.03 _{2.64-6.81}
MCD-0.1	.9885 _{.9803-0.9927}	.935 _{.828-0.962}	.838 _{.754-0.873}	.879 _{.600-0.943}	1.33 _{0.95-2.36}	1.36 _{1.07-2.21}	1.69 _{1.05-5.27}	2.87 _{1.78-5.42}	4.15 _{2.67-7.22}
MCD-0.5	.9876 _{.9751-0.9923}	.930 _{.808-0.960}	.819 _{.669-0.866}	.862 _{.508-0.939}	1.39 _{0.99-2.55}	1.46 _{1.12-2.85}	1.91 _{1.09-6.96}	3.22 _{1.91-6.71}	4.53 _{2.79-9.06}
Ensemble	.9892_{.9822-0.9930}	.941_{.859-0.965}	.847_{.773-0.878}	.907_{.716-0.953}	1.23_{0.90-2.03}	1.28_{1.01-1.97}	1.41_{0.93-3.70}	2.71_{1.73-4.72}	3.94_{2.59-6.67}
SSN	.9882 _{.9788-0.9926}	.934 _{.807-0.962}	.837 _{.736-0.871}	.860 _{.533-0.937}	1.31 _{0.95-2.48}	1.38 _{1.07-2.38}	1.83 _{1.11-6.51}	3.08 _{1.89-6.30}	4.36 _{2.74-8.05}

TABLE S5
P-VALUES FROM THE PAIRWISE WILCOXON SIGNED-RANK TEST COMPARING SEGMENTATION ACCURACY AND CALIBRATION OF DIFFERENT MODELS TRAINED ON THE UKBB DATASET AND TESTED ON THE ACDC DATASET (NS = NOT SIGNIFICANT, $p > 0.05$).

	Pixelwise Accuracy ↑	Dice ↑			ASSD (mm) ↓			NLL ↓ ($\times 10^{-2}$)	BS ↓ ($\times 10^{-3}$)
		LV	Myo	RV	LV	Myo	RV		
UKBB → ACDC									
Plain U-net vs BBB	<0.0001	<0.0001	<0.0001	<0.0001	<0.0001	<0.0001	<0.0001	<0.0001	<0.0001
Plain U-net vs MCD-0.1	<0.0001	<0.0001	<0.0001	0.0027	<0.0001	<0.0001	<0.0001	<0.0001	<0.0001
Plain U-net vs MCD-0.5	<0.0001	ns	<0.0001	<0.0001	<0.0001	<0.0001	<0.0001	ns	<0.0001
Plain U-net vs Ensemble	<0.0001	<0.0001	<0.0001	<0.0001	<0.0001	<0.0001	<0.0001	<0.0001	<0.0001
Plain U-net vs SSN	ns	<0.0001	0.0006	0.0006	<0.0001	<0.0001	ns	0.0002	ns
BBB vs MCD-0.1	<0.0001	<0.0001	<0.0001	0.0003	<0.0001	<0.0001	0.0002	<0.0001	<0.0001
BBB vs MCD-0.5	<0.0001	<0.0001	<0.0001	<0.0001	<0.0001	<0.0001	<0.0001	<0.0001	<0.0001
BBB vs Ensemble	<0.0001	ns	ns	<0.0001	ns	ns	<0.0001	<0.0001	<0.0001
BBB vs SSN	<0.0001	0.0074	<0.0001	<0.0001	0.0037	<0.0001	<0.0001	<0.0001	<0.0001
MCD-0.1 vs MCD-0.5	<0.0001	<0.0001	<0.0001	<0.0001	<0.0001	<0.0001	<0.0001	<0.0001	<0.0001
MCD-0.1 vs Ensemble	<0.0001	<0.0001	<0.0001	<0.0001	<0.0001	<0.0001	<0.0001	<0.0001	<0.0001
MCD-0.1 vs SSN	<0.0001	ns	ns	<0.0001	ns	ns	<0.0001	<0.0001	<0.0001
MCD-0.5 vs Ensemble	<0.0001	<0.0001	<0.0001	<0.0001	<0.0001	<0.0001	<0.0001	<0.0001	<0.0001
MCD-0.5 vs SSN	<0.0001	<0.0001	<0.0001	0.0009	<0.0001	<0.0001	<0.0001	ns	<0.0001
Ensemble vs SSN	<0.0001	ns	<0.0001	<0.0001	ns	<0.0001	<0.0001	<0.0001	<0.0001

TABLE S6
PREDICTIVE UNCERTAINTY MEASURES ON THE ACDC AND UKBB DATASETS USING MODEL TRAINED WITH UKBB DATASET. FORMAT: MEDIAN_{25-75TH PERCENTILE}

	Pred Entropy ($\times 10^{-2}$)	MI ($\times 10^{-3}$)	Dice _{ews}			ASSD _{ws}		
			LV	Myo	RV	LV	Myo	RV
UKBB → UKBB								
Plain U-net	1.03 _{0.77-1.33}	N/A	N/A	N/A	N/A	N/A	N/A	N/A
BBB	1.11 _{0.83-1.43}	0.32 _{0.24-0.43}	.990 _{.984-0.994}	.974 _{.964-0.979}	.982 _{.964-0.991}	0.214 _{0.167-0.273}	0.222 _{0.187-0.270}	0.286 _{0.200-0.432}
MCD-0.1	1.06 _{0.79-1.37}	0.09 _{0.06-0.13}	.995 _{.992-0.997}	.987 _{.982-0.989}	.991 _{.981-0.996}	0.099 _{0.071-0.137}	0.111 _{0.088-0.142}	0.142 _{0.091-0.238}
MCD-0.5	1.10 _{0.82-1.43}	0.16 _{0.11-0.29}	.994 _{.990-0.997}	.985 _{.979-0.988}	.988 _{.970-0.994}	0.116 _{0.083-0.162}	0.127 _{0.099-0.166}	0.188 _{0.117-0.372}
Ensemble	1.06 _{0.79-1.36}	0.22 _{0.16-0.34}	.993 _{.988-0.996}	.980 _{.971-0.985}	.985 _{.967-0.993}	0.159 _{0.113-0.219}	0.170 _{0.134-0.222}	0.245 _{0.155-0.404}
SSN	1.14 _{0.87-1.53}	2.89 _{2.11-5.24}	.971 _{.936-0.984}	.935 _{.895-0.947}	.914 _{.794-0.959}	0.554 _{0.408-0.851}	0.564 _{0.430-0.827}	1.113 _{0.725-2.826}
UKBB → ACDC								
Plain U-net	2.02 _{1.32-2.82}	N/A	N/A	N/A	N/A	N/A	N/A	N/A
BBB	2.35 _{1.55-3.55}	1.61 _{0.80-3.83}	.985 _{.964-0.991}	.961 _{.923-0.971}	.960 _{.840-0.984}	0.327 _{0.230-0.646}	0.353 _{0.254-0.668}	0.567 _{0.281-1.741}
MCD-0.1	2.15 _{1.42-3.18}	0.79 _{0.32-2.60}	.991 _{.974-0.995}	.975 _{.944-0.983}	.974 _{.876-0.991}	0.201 _{0.124-0.478}	0.231 _{0.146-0.514}	0.356 _{0.159-1.228}
MCD-0.5	2.53 _{1.60-4.15}	2.40 _{0.84-8.19}	.983 _{.925-0.993}	.956 _{.868-0.977}	.940 _{.755-0.984}	0.350 _{0.161-1.473}	0.396 _{0.192-1.549}	0.845 _{0.269-2.986}
Ensemble	2.30 _{1.50-3.63}	2.08 _{0.86-6.94}	.985 _{.948-0.992}	.957 _{.900-0.971}	.958 _{.814-0.986}	0.343 _{0.214-0.819}	0.390 _{0.242-0.938}	0.570 _{0.268-2.257}
SSN	2.36 _{1.53-3.61}	6.89 _{3.98-14.30}	.961 _{.878-0.981}	.917 _{.830-0.938}	.876 _{.731-0.947}	0.780 _{0.513-1.791}	0.744 _{0.536-1.654}	1.774 _{0.811-3.671}